

POST-CRASH FIRE FORENSIC ANALYSIS OF AEROSPACE COMPOSITES

A Thesis

by

HASNAA OUIDADI

Submitted to the Office of Graduate and Professional Studies of
Texas A&M University
in partial fulfillment of the requirements for the degree of

MASTER OF SCIENCE

Chair of Committee,	Thomas E. Lacy, Jr.
Committee Members,	Jaime Grunlan
	Qingsheng Wang
Head of Department,	Andreas A. Polycarpou

December 2020

Major Subject: Mechanical Engineering

Copyright 2020 Hasnaa Ouidadi

ABSTRACT

The primary goal of this research is to investigate the effects of fire exposure on thermal damage development in mechanically-failed graphite-epoxy composites. Vertical and horizontal fire tests were performed on mechanically-failed unnotched compression, short beam strength, and in-plane shear Cytec Cycom 5215 T40-800 graphite-epoxy specimens. In addition, a single cone calorimetry test was performed on a compression-after-impact specimen. Fire damage included melt dripping, matrix decomposition, char, soot, matrix cracking, delamination, and residual thickness increases due to explosive outgassing. Visual inspection and scanning electron microscopy of burned specimens showed that the specimen lay-up, specimen orientation relative to the heat source, and fracture surface morphology all had a significant influence on composite thermal degradation.

Thermal damage due to heat conduction, combustion, and/or thermal deformation was highly dependent on the ply orientation relative to the flame. Plies with fibers oriented *parallel* to the heat-exposed surface acted like a thermal protection layer that impeded (slowed) heat transfer to the interior of the specimen and promoted convection of hot gasses that *bypassed* the specimen. In contrast, plies with fibers oriented *perpendicular* to the heat-exposed surface (*i.e.*, burned parallel to the fibers) conducted heat into the interior of the composite, resulting in melt dripping, internal pockets of matrix decomposition, and surface char deposition that, in some cases, completely obscured salient aspects of fiber fracture surface morphology. Thermal

damage development in mechanically-failed laminates can be compounded by the presence of different ply groupings in a given stack-up, as well as the total available free surface area. Burned specimens with more free surface area sustained far more thermal degradation for a given fire exposure. Exposed fiber bundles were susceptible to severe thinning and thermal oxidation which destroyed key fractographic features.

To the author's knowledge, *this research is the first to investigate i) the effects of fire exposure on mechanically-failed continuous graphite fiber-epoxy laminates, and ii) the influence of specimen lay-up, orientation, and fracture surface morphology on different thermal degradation mechanisms in aerospace composites.* This research represents an important first step in the development of a coherent strategy for Federal Aviation Administration post-crash forensic analysis of composite aircraft structures.

ACKNOWLEDGEMENTS

I would like to express my sincere gratitude to my committee chair Dr. Thomas E. Lacy for his guidance, support, and advice throughout the course of this research and also for his valuable comments on this thesis. Thank you to my committee members, Dr. Jaime Grunlan, and Dr. Qingsheng Wang for letting us use their research labs to conduct the experimental work related to this thesis. Thank you to Dr. Charles U. Pittman for providing comments on this thesis. I also would like to thank the National Institute for Aviation Research for giving us the mechanically-failed graphite-epoxy specimens that were used in this work. Thanks to Simone Lazar, Thomas Kolibaba, Ruiqing Shen (Ryan), Dounia Boushab, Aniket Mote, Ashley Moody, and JD Leaverton for helping with part of the experimental work related to this thesis. Finally, I would like to address my special thanks to my parents, my family, and friends for their support and encouragement.

CONTRIBUTORS AND FUNDING SOURCES

Contributors

This work was supervised by a thesis committee consisting of Professor Thomas E. Lacy and Professor Jaime Grunlan of the Department of Mechanical Engineering and Professor Qingsheng Wang of the Department of Chemical Engineering.

Funding Sources

This work was made possible by the Federal Aviation Administration through Mississippi State University subcontract M1903125. Graduate study was also supported in part by teaching assistantships from Texas A&M University.

NOMENCLATURE

FAA	Federal Aviation Administration
GA	General aviation
IPS	In-plane shear
UNC0	Unnotched compression
SBS	Short beam strength
SEM	Scanning electron microscopy
WD	Working distance

TABLE OF CONTENTS

	Page
ABSTRACT	ii
ACKNOWLEDGEMENTS	iv
CONTRIBUTORS AND FUNDING SOURCES.....	v
NOMENCLATURE.....	vi
TABLE OF CONTENTS	vii
LIST OF FIGURES.....	ix
LIST OF TABLES	xiii
1. INTRODUCTION.....	1
1.1. Background.....	1
1.2. Fire Effects on Composite Materials	2
1.3. Motivation.....	10
1.4. Thermal-based Techniques for Char Removal from Aerospace Composites.....	13
2. SPECIMENS USED FOR BURNING TESTS.....	16
3. FIRE APPLICATION METHODS.....	19
3.1. Direct Fire Application Using a Bunsen Burner.....	19
3.1.1. Vertical Bunsen Burner Fire Tests	21
3.1.2. Horizontal Bunsen Burner Fire Tests	23
3.2. Fire Application Using Cone Calorimeter	24
4. TEST MATRIX.....	26
5. ANALYSIS OF MECHANICALLY-FAILED CYTEC CYCOM 5215 T40-800 GRAPHITE-EPOXY SPECIMENS SUBJECTED TO FIRE	28
5.1. Enclosed Vertical Fire Testing of Cytec Cycom 5215 T40-800 Graphite-epoxy Specimens.....	28
5.1.1. UNCO Specimens	28
5.1.2. SBS Specimens.....	41

5.1.3. IPS Specimens50

5.2. Enclosed Horizontal Fire Testing of Cytec Cycom 5215 T40-800 Graphite-epoxy
Specimens.....60

5.2.1. UNC0 Specimens60

5.2.2. SBS Specimens.....63

5.2.3. IPS Specimens67

5.3. Cone Calorimeter Testing of a Cytec Cycom 5215 T40-800 Graphite-epoxy
Compression-after-impact (CAI) Specimen.....71

6. SUMMARY AND CONCLUSIONS.....78

REFERENCES85

LIST OF FIGURES

	Page
Figure 1.1 Schematic of the reaction processes in the through-thickness direction of a hot, decomposing polymer composite during fire exposure (Reprinted with permission from [10]).	4
Figure 1.2 Photographs of a woven E-glass/polyester composite cross-section after being exposed to a heat flux of 50 kW/m ² for (a) 0, (b) 85, (c) 325, and (d) 1800 s, respectively. The composite was 11.5 mm thick and did not have a thermal barrier coating. The upper surface was exposed to the heat source (Reprinted with permission from [8]).	7
Figure 1.3 (a) Schematic diagram showing the different fire-damaged regions through the thickness of the composite. Scanning electron micrographs of the (b) char layer, (c) interface between the char layer and unburned composite, (d) delamination cracks, and (e) a resin-rich region in the unburned composite (Reprinted with permission from [8]).	9
Figure 1.4 SEM images of a 21-ply cross-ply Cytec Cycom 5215 T40-800 graphite-epoxy specimen failed in compression; (a) before and (b) after 36 s vertical burning (WD = 9 mm).	13
Figure 3.1 Draft-free cabinets that meet the FAA fire testing requirements.	19
Figure 3.2 Burner plumbing and burner flame height indicator (Reprinted from [19]).	20
Figure 3.3 Schematic of specimen positioning with respect to the flame (a) for vertical fire tests and (b) horizontal fire tests (Adapted from [19]).	21
Figure 3.4 Picture of a 21-ply cross-ply Cytec Cycom 5215 T40-800 graphite-epoxy UNCO specimen during vertical burning test using a Bunsen burner.	22
Figure 3.5 Picture of a 21-ply cross-ply Cytec Cycom 5215 T40-800 graphite-epoxy UNCO specimen during horizontal burning test using a Bunsen burner.	23
Figure 3.6 A schematic view of a cone calorimeter (Reprinted with permission from [20]).	25
Figure 5.1 Fire sparkles during the 12 s vertical burn test on a 21-ply cross-ply Cytec Cycom 5215 T40-800 graphite-epoxy UNCO specimen.	30
Figure 5.2 Pictures of a 21-ply cross-ply Cytec Cycom 5215 T40-800 graphite-epoxy UNCO specimen; (a) before and (b) and (c) after vertical burning for 60 s.	32

Figure 5.3 SEM images showing char and soot deposition around the perimeter of the fracture surface of 21-ply cross-ply Cytec Cycom 5215 T40-800 graphite-epoxy UNC0 specimens burned vertically for (a) 12, (b) 36, and (c) 60 s.....	33
Figure 5.4 SEM images showing the fuzzy (cotton-candy-like) appearance of char formed around single fibers in 21-ply cross-ply Cytec Cycom 5215 T40-800 graphite-epoxy UNC0 specimens burned vertically for (a) 12, (b) 36, and (c) 60 s.	34
Figure 5.5 Fracture characteristics on (a) a 21-ply cross-ply Cytec Cycom 5215 T40-800 graphite-epoxy UNC0 specimen before burning, and on recessed fibers on specimens of the same failure modes after vertical burning for (b) 12, (c) 36, and (d) 60 s.	37
Figure 5.6 Micro-buckling terraces on compression failed CFRP specimen (x700) (Adapted with permission from [23]).	38
Figure 5.7 SEM image showing micro-buckled fibers in a 21-ply cross-ply Cytec Cycom 5215 T40-800 graphite-epoxy UNC0 specimen burned vertically for 60 s.....	38
Figure 5.8 (a) Melt dripping on fracture fibers ends of a 21-ply cross-ply Cytec Cycom 5215 T40-800 graphite-epoxy UNC0 specimen burned vertically for 36 s (b) a magnified view of filaments covered with melt dripping.....	39
Figure 5.9 Delamination in a 21-ply cross-ply Cytec Cycom 5215 T40-800 graphite-epoxy UNC0 specimen burned vertically for 60 s.....	40
Figure 5.10 Matrix cracking in a 21-ply cross-ply Cytec Cycom 5215 T40-800 graphite-epoxy UNC0 specimen burned vertically for 60 s.	40
Figure 5.11 Picture of a 45-ply unidirectional Cytec Cycom 5215 T40-800 graphite-epoxy SBS specimen; (a) before and (b) after vertical burning for 60 s.	42
Figure 5.12 SEM images showing char and soot deposition on the fracture surface of 45-ply unidirectional Cytec Cycom 5215 T40-800 graphite-epoxy SBS specimens after vertical burning for (a) 12, (b) 36, and (c) 60 s.	44
Figure 5.13 SEM images showing the fuzzy (cotton-candy-like) appearance of char formed around single fibers in 45-ply unidirectional Cytec Cycom 5215 T40-800 graphite-epoxy SBS specimens burned vertically for (a) 36, and (b) 60 s.	45
Figure 5.14 Fracture characteristics on (a) a 45-ply unidirectional SBS Cytec Cycom 5215 T40-800 graphite-epoxy specimen before burning, and on recessed	

fibers on specimens of the same failure modes after vertical burning for (b) 12, (c) 36, and (d) 60 s.	48
Figure 5.15 Micro-buckled fibers in Cytec Cycom 5215 T40-800 graphite-epoxy SBS specimens: (a) unburned specimen, (b) magnified view of the unburned specimen, and (c) specimen vertically burned for 60 s.	49
Figure 5.16 Micro-buckled fibers in Cytec Cycom 5215 T40-800 graphite-epoxy SBS specimens completely covered in melt dripping.	50
Figure 5.17 Positioning of the IPS specimen during vertical burn tests.	52
Figure 5.18 Pictures of a 16-ply Cytec Cycom 5215 T40-800 graphite-epoxy IPS specimen (a) before and (b) and (c) after vertical fire exposure for 6 s. In (a), locations 1, 2, and 3 denote the longest lateral edge, laminate centerline, and shortest lateral edge, respectively.	53
Figure 5.19 SEM micrographs showing char and soot deposition on fractured fibers located at (a) the longest lateral edge, (b) center and (c) shortest lateral edge of 16-ply Cytec Cycom 5215 T40-800 graphite-epoxy IPS specimens subjected to 6 s vertical burn test. These correspond to locations 1, 2, and 3, respectively, in Figure 5.18a.	54
Figure 5.20 SEM images showing char formation on (a) the longest and (b) shortest lateral edges of 16-ply Cytec Cycom 5215 T40-800 graphite-epoxy IPS specimens burned vertically for 12 s both taken at a WD of 15 mm. These correspond to locations 1 and 3 in Figure 5.18a.	56
Figure 5.21 SEM images showing char formation on (a) the longest and (b) shortest lateral edges of 16-ply Cytec Cycom 5215 T40-800 graphite-epoxy IPS specimens burned vertically for 36 s taken at WDs of 9 and 11 mm, respectively. These correspond to locations 1 and 3 in Figure 5.18a.	56
Figure 5.22 SEM images showing char formation on (a) the longest and (b) shortest lateral edges of 16-ply Cytec Cycom 5215 T40-800 graphite-epoxy IPS specimens burned vertically for 60 s taken at WDs of 12 and 25 mm, respectively. These correspond to locations 1 and 3 in Figure 5.18a.	57
Figure 5.23 Fiber-end thinning of filaments located at the mid-plane of 16-ply Cytec Cycom 5215 T40-800 graphite-epoxy IPS specimens vertically burned for (a) 12, (b) 36 and (c) 60 s taken at WDs of 9, 15, and 10 mm, respectively.	59
Figure 5.24 SEM image showing voids and cavities on a fiber from a 16-ply Cytec Cycom 5215 T40-800 graphite-epoxy IPS specimen burned vertically for 60 s.	60

Figure 5.25 Pictures of a 21-ply cross-ply Cytec Cycom 5215 T40-800 graphite-epoxy UNCO specimen; (a, c) before and (b, d) after horizontal burning for 75 s.....	61
Figure 5.26 SEM image of the char and soot deposition at the fracture surface of a 21-ply cross-ply Cytec Cycom 5215 T40-800 graphite-epoxy cross-ply UNCO specimen used on 15 s horizontal fire test.	63
Figure 5.27 Pictures of a 45-ply unidirectional Cytec Cycom 5215 T40-800 graphite-epoxy SBS specimen; (a, c) before and (b, d) after horizontal burning for 75 s.....	65
Figure 5.28 SEM image showing char and soot deposition at the fracture surface of 45-ply unidirectional Cytec Cycom 5215 T40-800 graphite-epoxy SBS specimens used for (a) 15, (b) 45, and (c) 75 s horizontal fire tests.....	66
Figure 5.29 Pictures of a 16-ply Cytec Cycom 5215 T40-800 graphite-epoxy IPS specimen; (a, c) before and (b, d) after horizontal burning for 75 s; “x” denotes the approximate location of the axis of the vertical flame.	68
Figure 5.30 SEM images showing fiber tows from the centerline of 16-ply Cytec Cycom 5215 T40-800 graphite-epoxy IPS specimens after horizontal burning for (a) 15, (b) 45, and (c) 75 s.	70
Figure 5.31 Cone calorimetry testing of a 4 x 4 in ² 32-ply Cytec Cycom 5215 T40-800 graphite-epoxy CAI specimen.	74
Figure 5.32 (a) 4 x 4 in ² 32-ply Cytec Cycom 5215 T40-800 graphite-epoxy CAI specimen after cone calorimeter fire testing using a heat flux of 50 kW/m ² , (b) zoomed-in picture of the specimen showing loose fibers (c) zoomed-in picture of the specimen showing edge delamination.....	76
Figure 5.33 Melt dripping from the 4 x 4 in ² 32-ply Cytec Cycom 5215 T40-800 graphite-epoxy CAI specimen.	77

LIST OF TABLES

	Page
Table 1.1 Typical Fracture Characteristics for Different Failure Modes (Reprinted from [14]).....	12
Table 2.1 Number of Plies, Lay-up, and Typical Picture of the UNC0, SBS and IPS Specimens (Adapted from [18]).	18
Table 4.1 Summary of Mechanically-failed Specimens Subjected to Fire Testing.	27

1. INTRODUCTION

1.1. Background

Typical continuous fiber aerospace composite materials have many advantageous mechanical and thermal properties over metals. They are lightweight, corrosion-resistant, can take complex shapes and have low maintenance and manufacturing costs [1]. In addition, fiber-reinforced composite materials can offer better fatigue resistance than metals. The high stiffness and strength of continuous fibers facilitate fiber-crack bridging that mitigates the nucleation and growth of matrix cracks and improves fatigue properties [2]. As a result, the use of composite materials in primary structural applications has increased dramatically over the past decades. They are now used in aerospace, automotive, and many other high-tech and low-tech applications that require high stiffness/weight and/or strength/weight ratios. Despite their high specific properties, composite materials often suffer from relatively high moisture absorption and low fracture toughness [2]. Moreover, their structural performance and damage tolerance degrade at elevated temperatures [3, 4].

Although continuous-fiber carbon-epoxy composite materials for aerospace applications provide high specific mechanical and thermal properties, their use should not affect the post-fire safety already assured by aluminum aircraft [5]. The aluminum lower wing panels used on commercial passenger aircraft wings have been certified as being fire-resistant over a wide range of typical skin thicknesses. Use of aluminum skins can also lessen the risk of fuel tank explosion in the case of a fuel-fed external fire, due to its high thermal conductivity [5]. A similar understanding of the fire

resistance of composite aircraft structures is very crucial, especially since they are increasingly used as an alternative to metals in commercial aircraft, general aviation (GA) aircraft, and unmanned aerial system primary structures.

Compared to metallic aircraft structures, carbon-epoxy composite structures can have low thermal conductivities which can affect heat transfer and spread of a flame in the event of a fire [3]. However, due to their organic matrix (and sometimes fibers) they are very prone to react with fire [3, 6]. When an epoxy matrix (thermoset) composite material is exposed to elevated temperatures that are *below* the resin curing temperature, the polymer matrix softens, increasing the likelihood of instability or matrix-dominated failures and loss of aircraft structural integrity. Once the resin curing temperature is exceeded, thermosetting matrices will further cure, decompose, and start reacting with the fire (combustion). At extremely high temperatures encountered during aircraft fires, the organic components of the composite structures (*i.e.*, matrices and fibers) start decomposing, leading to the generation of toxic smoke and gases. In addition, the decomposition of these organic parts leads to the formation and deposition of char and other fire by-products on the burned composite surfaces [3, 4]. Moreover, thermally-induced large-scale matrix decomposition, fiber ablation/sublimation, and delamination due to fire exposure can result in significant decreases in composite moduli and strengths [3, 6-10].

1.2. Fire Effects on Composite Materials

Fire damage in continuous-fiber-reinforced composite materials involves the concurrent and sequential interaction between many complex physical, chemical,

thermal, and failure processes [10]. The physical processes include constituent material expansion and contraction, ply-delamination, matrix cracking, and the formation of high-pressure regions due to matrix outgassing. The chemical processes involve the phase changes that occur inside the composite material, including the softening, melting, and decomposition of the matrix, as well as char formation and growth. The thermal processes involve the evolving temperature distributions, heat transfer through the material due to conduction, convection of the gases formed during the decomposition, and pyrolysis of the polymeric matrix and organic fibers. Lastly, the failure processes involve the permanent degradation of the mechanical properties of the composites and failure of the load-carrying capability of the composite structures due to fire [3, 10]. Figure 1.1 (reprinted with permission from [10]) shows a schematic of the reaction processes in the through-thickness direction of a hot, decomposing polymer composite during fire exposure.

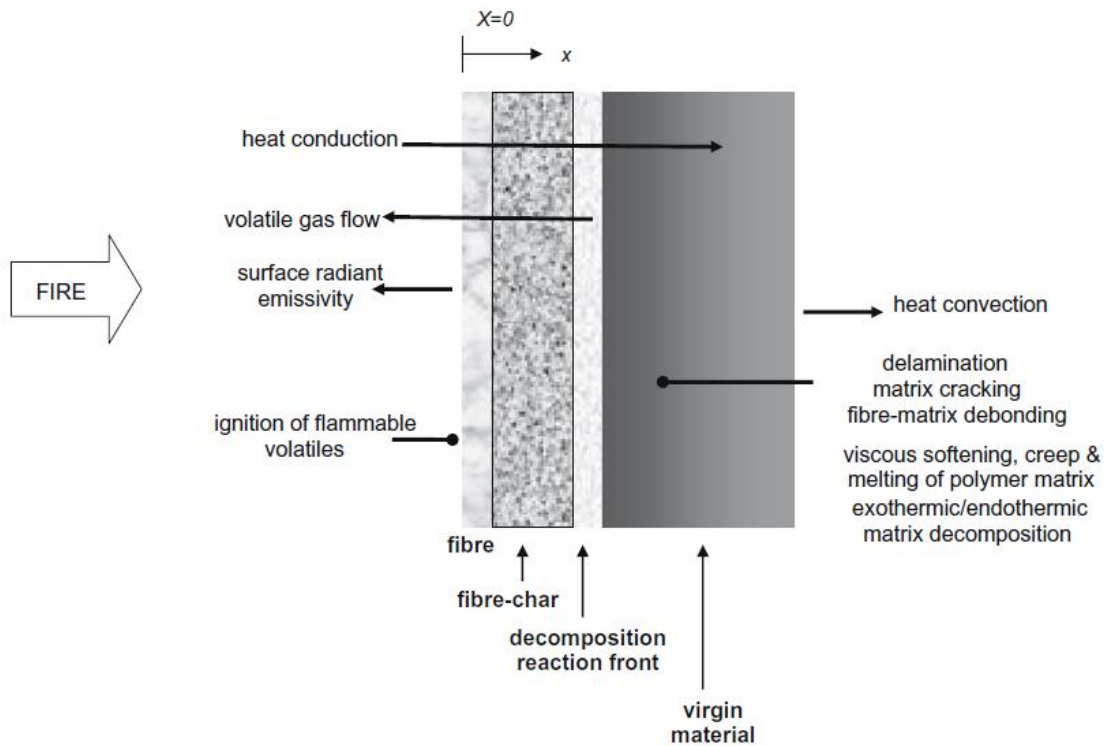


Figure 1.1 Schematic of the reaction processes in the through-thickness direction of a hot, decomposing polymer composite during fire exposure (Reprinted with permission from [10]).

When a mechanically-failed composite material specimen is subsequently exposed to a fire or a heat flux, the elevated temperature at the exposed fractured surface leads to significant localized heat conduction within the specimen. As the local temperature initially increases, the resulting matrix softening can contribute to a variety of matrix-dominated instability failures that can jeopardize aircraft structural integrity. Once the increasing temperature exceeds the thermoset resin curing temperature, the matrix will further cure and then decompose leading to char formation and the generation of smoke, toxic gases, and vaporized moisture [3, 6]. Due to the initial low permeability and porosity of typical aerospace composites,

combustion-induced gases trapped inside vacancies (voids) created during burning result in matrix regions with very high internal local pressures. These voids can eventually rupture, leading to extreme ply-delamination and a significant increase in residual laminate thickness after fire exposure [3, 6, 10]. In addition, expanding hot gasses from matrix outgassing dramatically increase convective heat transfer through the specimen and spread decomposed matrix residues over fire/heat-exposed composite surfaces. Such residues contribute to the deposition of solid carbonaceous soot and char on the fractured surface, which can obscure salient aspects of failure surface morphology necessary to identify operative mechanical failure mechanisms. One key aspect of this thesis is to characterize how varying levels of fire exposure alter aerospace composite failure surfaces in order to facilitate post-fire forensic analysis.

The degree and amount of char formation highly depend on both the original polymer matrix and organic fibers [3]. Char structures consist of 85-98% carbon and particles of aromatic-aliphatic compounds often with heteroatoms such as oxygen (O), phosphorus (P), nitrogen (N), and sulfur (S). Depending on the fire environment, temperature, and also the chemical composition of the polymer matrix and organic fibers, char can contain crystalline and/or amorphous regions [3]. Char can vary in composition from melted and partly oxidized matrix (resin) all the way to a highly carbonized material.

Due to its low thermal conductivity, char formed at the exposed surface of the burned composite material may serve as a protective layer that impedes further

burning [3]. Mouritz and Mathys [8] used cone calorimetry to investigate the effect of through-thickness heat flux and fire exposure duration on the char formation in an 11.5 mm thick E-glass woven roving fabric and an isophthalic polyester composite laminate. Figure 1.2 (reprinted with permission from [8]) shows the cross-section of the woven composite after being exposed to an upper surface heat flux of 50 kW/m^2 for four different time periods: (a) 0, (b) 85, (c) 325, and (d) 1800 s. As shown in the figure, the char layer thickness increased with the increase in heat flux exposure duration. Moreover, the char developed through the entire 11.5 mm specimen thickness (Figure 1.2d) due to the total thermal decomposition and combustion of the polyester matrix.

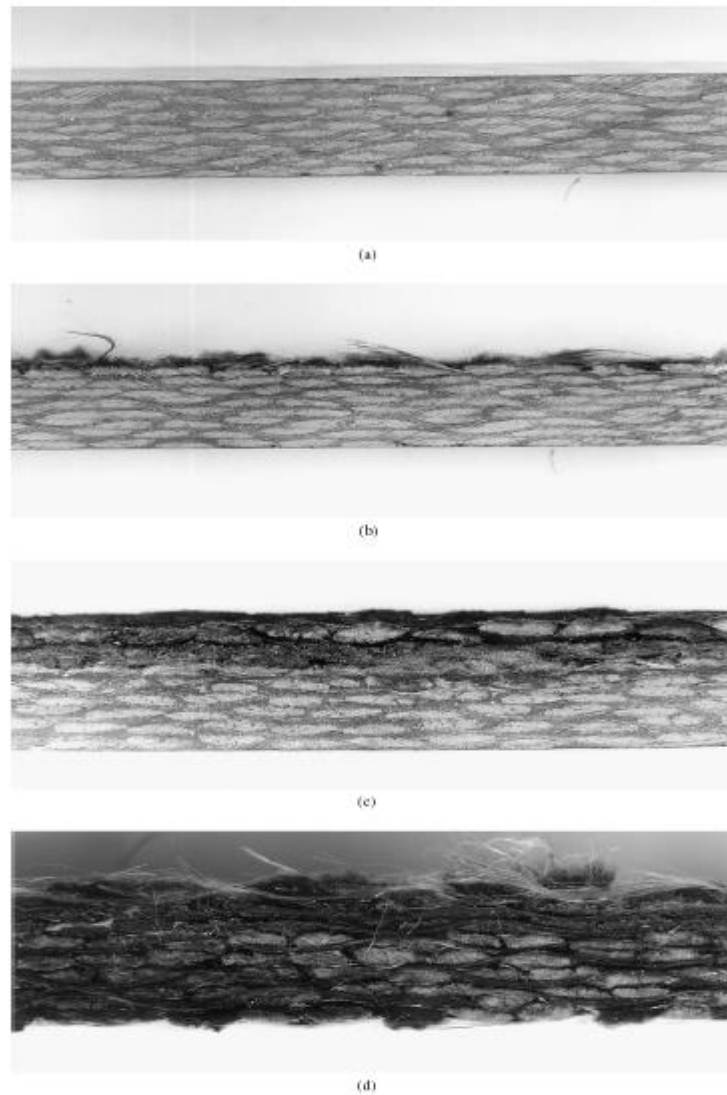


Figure 1.2 Photographs of a woven E-glass/polyester composite cross-section after being exposed to a heat flux of 50 kW/m^2 for (a) 0, (b) 85, (c) 325, and (d) 1800 s, respectively. The composite was 11.5 mm thick and did not have a thermal barrier coating. The upper surface was exposed to the heat source (Reprinted with permission from [8]).

Mouritz and Mathys [8] also showed that the rate of char formation was independent of the heat flux. Exothermic decomposition of the polyester matrix enhanced the combustion process upon the ignition of the composite. However, the

char growth rate depended on the post-ignition heat-exposure time and the rate of oxygen transfer to the combustion front. The combustion front is defined as the interface between the burned and unburned layers of the composite. The oxygen transport rate dropped as the char thickness increased [8], leading to a decrease in the char formation rate.

In general, composite fire damage involves extensive matrix thermal decomposition, soot deposition, char formation, severe fire-induced delamination, matrix cracking, residual thickness increases, and fiber-matrix debonding [3, 10]. Scanning electron microscopy (SEM) images of the fire damage induced in an E-glass woven roving fabric and an isophthalic polyester composite are presented in Figure 1.3 (reprinted with permission from [8]). Figure 1.3a shows a through-thickness schematic of the fire damage in the specimen. Figures 1.3b, e show representative SEM images of the char layer, an interfacial region (combustion front) between the char layer and unburned composite, delamination cracks, and a matrix-rich region in the unburned part of the composite, respectively. The char region (Figure 1.3b) was primarily comprised of burned fibers since the matrix was mostly decomposed. In the combustion front (Figure 1.3c), many fibers displayed longitudinal cracking and were generally detached from the matrix. Delamination occurred between the underlying unburned layers. The delamination was assumed to be due to the significant difference in thermal conductivities (and coefficients of thermal expansion) between the charred layer and underlying composite layers.

Finally, the unburned region of the composite thermally degraded and contained some matrix-rich pockets [8].

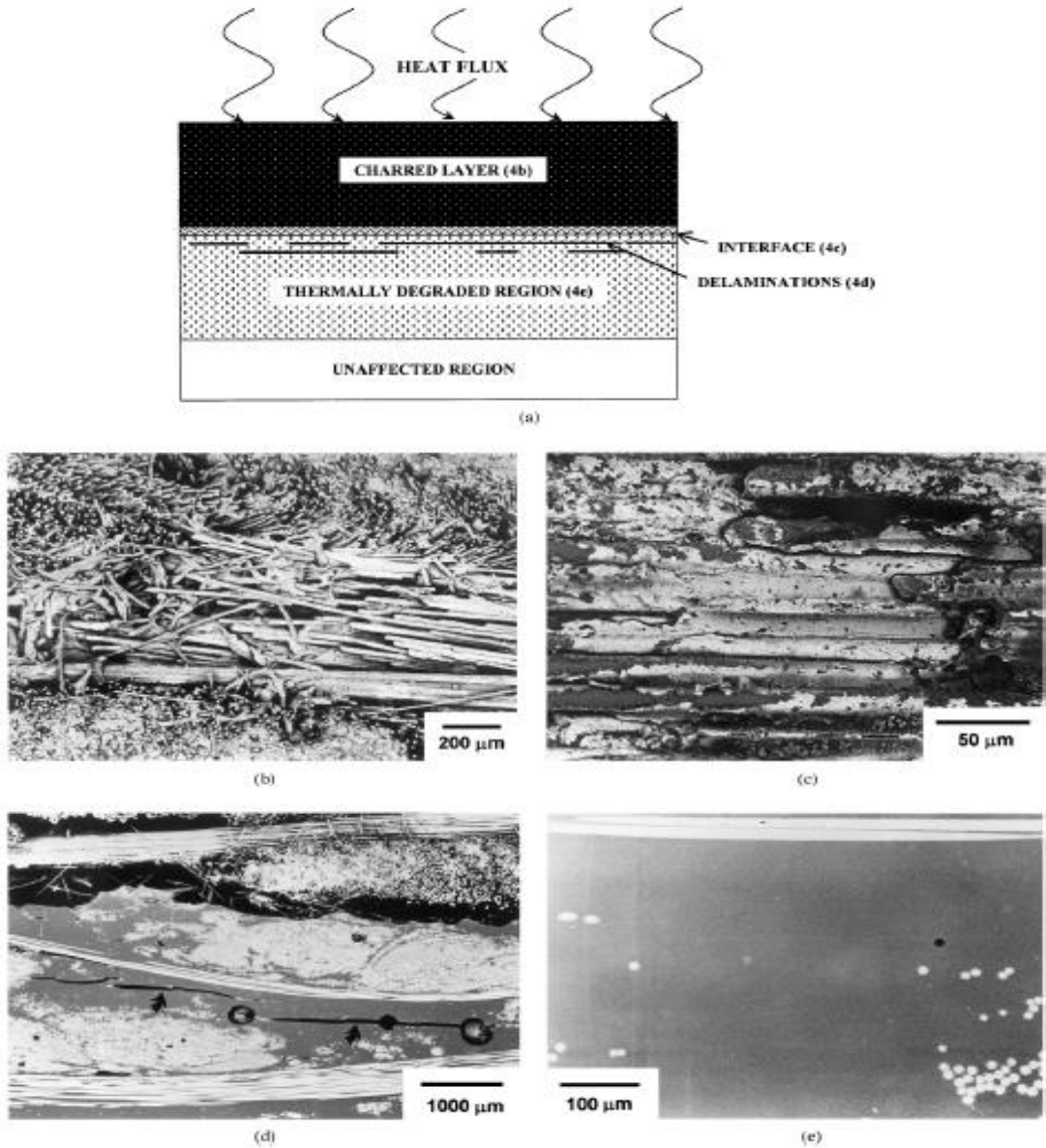


Figure 1.3 (a) Schematic diagram showing the different fire-damaged regions through the thickness of the composite. Scanning electron micrographs of the (b) char layer, (c) interface between the char layer and unburned composite, (d) delamination cracks, and (e) a resin-rich region in the unburned composite (Reprinted with permission from [8]).

1.3. Motivation

The causes of *in-flight* fires are well understood and the Federal Aviation Administration (FAA) and other aviation authorities have set strict fire safety standards. As a consequence, in-flight fires on commercial and GA aircraft are very uncommon [3]. Non-fire related aircraft crashes, however, can result in major post-crash fires on the ground. For example, after an aircraft crash, fuel tank ruptures may allow direct contact between fuel and ignition sources (electrical circuits, engines, *etc.*) [11].

Post-crash fires involving composite aircraft structures are very undesirable for two main reasons. First, burning composites can generate thick toxic gases and smoke that can delay and jeopardize aircraft evacuation, as well as pose a serious health risk to passengers and emergency personnel [3]. Second, post-crash fires can dramatically alter the exposed surfaces of mechanically-failed structures in ways that inhibit post-crash forensic analysis and impede accident reconstruction analyses. The latter issue is the primary focus of this thesis. In essence, the formation of char and other thermal by-products due to post-crash fires can mask relevant aspects of the structural damage morphology and other evidence necessary to identify the underlying failure mechanisms that caused the crash [11, 12].

Similar to metals, composite failure surface fractography can be used to identify operative failure mechanisms that are crucial for post-crash forensic analyses and aircraft accident reconstruction [13]. Each relevant failure mode (interlaminar tension, interlaminar shear, translaminar tension, translaminar compression,

translaminar flexure, *etc.*) has specific macroscopic and microscopic fractographic features. Here, “interlaminar” is used to connote failures between plies, whereas “translaminar” refers to axial failures in the local fiber direction (fracture, micro-buckling, *etc.*). Table 1.1 (reprinted from [14]) summarizes typical fracture characteristics for different laminated composite material failure modes.

When fractured composite specimens are exposed to extremely high temperatures due to fire or elevated heat fluxes, the char and other carbonaceous residues deposited on the fracture surface and broken fiber ends can mask key features (*cf.*, Table 1.1) necessary to characterize the nature of the original mechanical failure. For instance, Figure 1.4 compares SEM images before and after the burning of a 21-ply cross-ply Cytec Cycom 5215 T40-800 graphite-epoxy specimen failed in compression. Prior to fire exposure (Figure 1.4a), the characteristic compressive fracture surface features are clearly visible. These include: *i*) “chop” marks on broken fiber surfaces that demarcate the transition between tensile and compressive failure in individual fibers (*i.e.*, neutral axis), and *ii*) matrix debris at the fractured surface. These critical features can be obscured or destroyed after fire exposure. For example, large-scale char formation on the broken fiber ends and extensive matrix decomposition (Figure 1.4b) impede traditional fractographic assessments of mechanical failure. One *long*-term goal of this FAA-sponsored research is to investigate techniques for char removal that will enable identification of relevant mechanical failure mechanisms, as well as facilitate forensic analysis of composites exposed to post-crash fires. As an important first step in reaching the FAA’s goal, this

MS thesis research aims to clarify the mechanisms responsible for thermal damage and char formation in mechanically-failed aerospace composite specimens.

Table 1.1 Typical Fracture Characteristics for Different Failure Modes (Reprinted from [14]).

Failure Mode	Macroscopic Features	Microscopic Features
Interlaminar¹ Tension	<ul style="list-style-type: none"> • Smooth, glassy fracture surface 	<ul style="list-style-type: none"> • Smooth surface • River marks • Resin microflow
Interlaminar Shear	<ul style="list-style-type: none"> • Flat surface, but with milky appearance under oblique lighting 	<ul style="list-style-type: none"> • Rough surface • Straight parallel hackle marks
Translaminar² Tension	<ul style="list-style-type: none"> • Rough, jagged fracture surface with individual fibers protruding from the surface 	<ul style="list-style-type: none"> • Fiber end fracture, pullout • Radial marks at the fiber ends
Translaminar Compression	<ul style="list-style-type: none"> • Extreme surface damage; very few fibers protruding from the surface 	<ul style="list-style-type: none"> • Fiber micro-buckling for thin laminate. Fiber ends show radial topology (tension) and smooth/ratcheted topology (compression), with a neutral axis • Fiber ends with slanted shear type failure for thick laminate
Translaminar Flexure	<ul style="list-style-type: none"> • Two distinct regions, exhibiting translaminar tension and compression, respectively, separated by a neutral axis 	<ul style="list-style-type: none"> • Both translaminar tension and compression features

¹ Interlaminar is used to connote failures between plies.

² Translaminar refers to axial failures in the local fiber direction (fracture, micro-buckling, *etc.*).

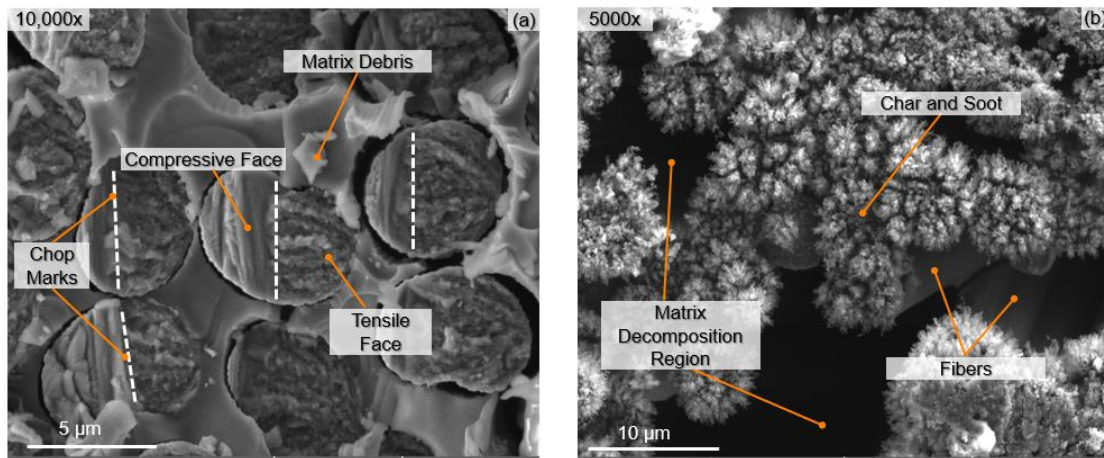


Figure 1.4 SEM images of a 21-ply cross-ply Cytec Cycom 5215 T40-800 graphite-epoxy specimen failed in compression; (a) before and (b) after 36 s vertical burning (WD = 9 mm).

1.4. Thermal-based Techniques for Char Removal from Aerospace Composites

A number of thermal-based techniques exist for removing cured thermosetting matrices from the surrounding fiber preforms [15-17]. For carbon-epoxy composites, these include standard “matrix ignition” approaches for fiber volume fraction determination [15], as well as approaches aimed at recycling carbon fibers from discarded thermoset composites [16, 17]. Such approaches may prove useful in removing char, melt dripping, and other fire by-products from carbon filament ends in a manner that aids fractographic assessments of broken fibers. In matrix ignition techniques, the thermoset matrix is completely burned off, which allows visual examination of the fibers and laminate architectures [15]. The ASTM standard ignition loss test method for cured reinforced thermoset resins [15] is used to determine the mass fraction of matrix and fiber. Essentially, a crucible is heated to

500-600°C for 10 min or more, cooled at room temperature, and then weighed to the nearest 1.0 mg [15]. A composite specimen is placed in the crucible, and the specimen/crucible combination is weighed. The crucible is heated in an open flame using a Bunsen burner until complete combustion of the specimen matrix occurs, and only ash and carbon fibers remain. The filled crucible is then reheated in a furnace at 565°C to remove all the carbonaceous residues due to initial burning. The duration of each heating step is highly dependent on the sample geometry. Finally, the sample and crucible are cooled to room temperature inside a desiccator and then weighed to assess mass loss due to matrix ignition [15].

Similar pyrolysis-based techniques are used to recycle carbon fibers in a manner that does not damage the fiber surfaces [16, 17]. Such processes involve the thermo-chemical decomposition of a composite organic matrix at temperatures in the range of 450-700°C in an inert environment [16]. The temperature levels are dependent on the thermosetting matrix. For polyester matrix and epoxy matrix composites, pyrolysis reactions are performed at 450°C and up to 550°C, respectively [17]. Due to the high pyrolysis temperatures, char is deposited on the surface of the recycled fibers [16]. As a consequence, pyrolysis is usually combined with an oxidation process to remove char and obtain clean fibers. The coupled pyrolysis/oxidation is performed using specialized thermolysis equipment, which consists of a heating system (for pyrolysis) and a gas condensation device (for oxidation). The oxidation time should be carefully optimized to avoid degradation of

the carbon fibers [16]. While not part of this thesis, thermal-based approaches appear to be promising techniques for char removal from aerospace composites.

2. SPECIMENS USED FOR BURNING TESTS

In this study, previously failed unnotched compression (UNC0), short beam strength (SBS), in-plane shear (IPS) Cytec Cycom 5215 T40-800 graphite-epoxy specimens [18] were subjected to direct fire testing using a Bunsen burner inside draft-free cabinets. One primary goal of this work was to investigate the effect of specimen geometry, failure surface morphology, and failure modes on char formation and other fire-induced thermal damage. The fire tests were conducted for different fire exposure durations and specimen orientations during burning (*i.e.*, vertical versus horizontal configurations). After mechanical testing, any failed UNC0, SBS, and IPS specimens that were not completely severed were separated into two distinct halves.




Table 2.1 (adapted from [18]) presents the number of plies, lay-up, and a typical laboratory-scale picture of an unburned half-sample for each of the UNC0, SBS, and IPS graphite-epoxy specimens. When compared to angle-ply laminates subjected to off-axis loadings (*i.e.*, IPS specimens), the failed UNC0 and SBS specimens generally had more compact failure surfaces with far less free surface area creation. Mechanical damage in UNC0 and SBS specimens tended to be concentrated in a planar damage zone oriented perpendicular to the longitudinal axis of the specimens. For $[90/0/90]_7$ UNC0 specimens subjected to uniaxial compression parallel to the 0° fibers, the damage zone contained a number of instability-related failures including micro-buckled/fractured 0° fibers, small kink bands, micro-buckling “terraces,” matrix fracture/crushing in 90° plies, and small-scale delamination between plies. For $[0]_{45}$ SBS three-point flexure specimens, the damage zone can be

divided into two distinct failure regions associated with translaminar tension and compression, separated by a neutral axis; damage included tensile fiber fractures, fiber pullouts, matrix cracking, micro-buckled fibers, large kink bands, and micro-buckling terraces. The UNCO and SBS specimens both contained large numbers of individual broken fiber ends that were either *extended* beyond the fracture surface or *recessed* within the composite. Such failures are consistent with classical fiber pullout behavior where there is a spatial distribution of strength values along each filament length. Moreover, extended or recessed filaments may differ in their susceptibility to direct fire exposure due to the presence (or lack) of surrounding matrix, airflow, and availability of oxygen. In contrast, IPS specimen failure was more widespread and diffuse, with far more free surface area generated than for UNCO and SBS specimens. Mechanical damage consisted of multiple translaminar fractures of individual $\pm 45^\circ$ plies with a non-uniform distribution of ply fracture planes along the specimen gage section, longitudinal splitting of fiber tows, and large-scale ply-delamination.

As an aside, the 21-ply cross-ply UNCO specimens and 45-ply unidirectional SBS specimens are somewhat consistent with thicker aerospace composite principal structural elements (primary axial load carrying members such as critical wing spars flanges, longerons, carry-through structures, *etc.*). The 16-ply IPS specimens are more consistent with thinner laminates designed to carry torsional and/or shear loads (wing skins, spar webs, *etc.*). In a post-crash forensic analysis of aerospace composites, special consideration is given to failed principal structural elements since they can be associated with the loss of an aircraft. Hence, an understanding of how the number of

plies, total stack-up thickness, lay-up, and mechanical failure surface morphology affect subsequent fire damage development in aerospace composites is crucial for successful post-crash fire forensics.

Table 2.1 Number of Plies, Lay-up, and Typical Picture of the UNC0, SBS and IPS Specimens (Adapted from [18]).

Specimen	Number of Plies	Lay-up	Typical Picture Before Burning
UNC0	21	[90/0/90] ₇	
SBS	45	[0] ₄₅	
IPS	16	[45/-45] _{4S}	

3. FIRE APPLICATION METHODS

3.1. Direct Fire Application Using a Bunsen Burner

The FAA has defined vertical and horizontal Bunsen burner test protocols [19] to address fire tests specified in the Federal Aviation Regulation (FAR) 25.853 and FAR 25.855. These protocols are used to verify the fire resistance of aircraft cabin and cargo compartment materials. Draft-free cabinets that meet the FAA fire test requirements were used to conduct vertical and horizontal Bunsen burner tests in accordance with the FAR 25.853 (Figure 3.1).

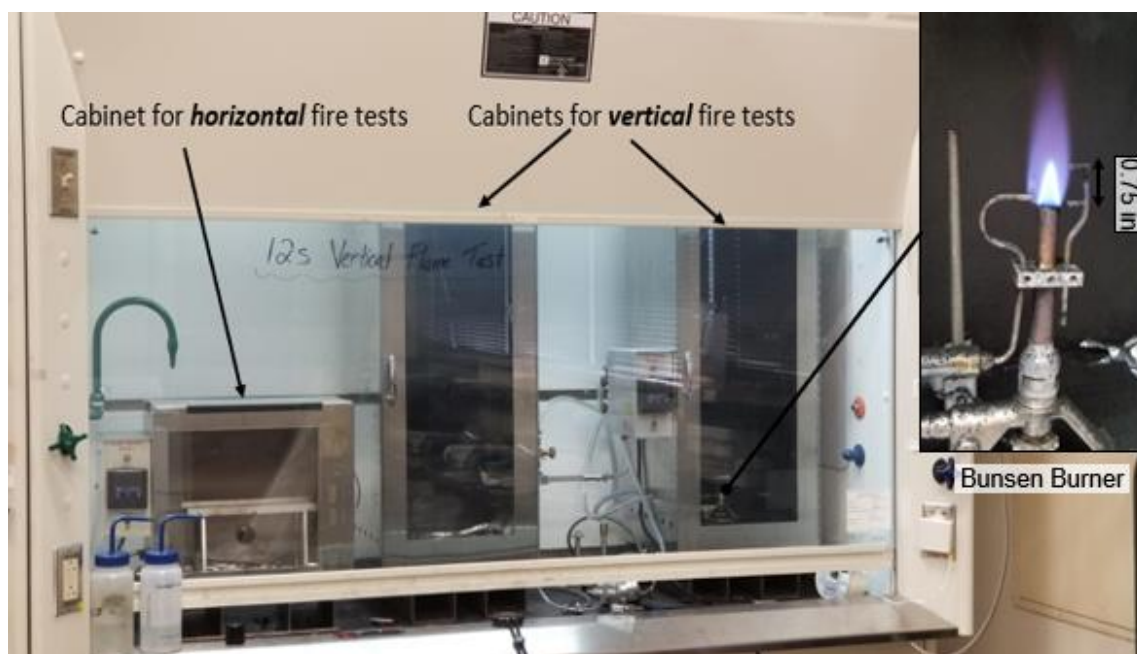


Figure 3.1 Draft-free cabinets that meet the FAA fire testing requirements.

Figure 3.2 (reprinted from [19]) shows a schematic of the burner plumbing and burner flame height indicator used for both the horizontal and vertical burning test configurations. Following the FAA recommendations, all burning tests were

performed using methane fuel and an optimal flame profile consisting of an inner cone height of $\frac{7}{8}$ in and flame tip height of 1.5 in (Figure 3.2). During the burning tests, the fractured specimen ends were completely immersed in the flame with a standoff distance of $\frac{3}{4}$ in from the edge of the burner. Consistent with the FAA Bunsen burner protocol, this standoff distance puts the fractured surface of the specimen at the top of the inner (blue) cone of the flame [19]. Figures 3.3a, b (adapted from [19]) show schematics of specimen positioning with respect to the flame for (a) vertical fire tests and (b) horizontal fire tests.

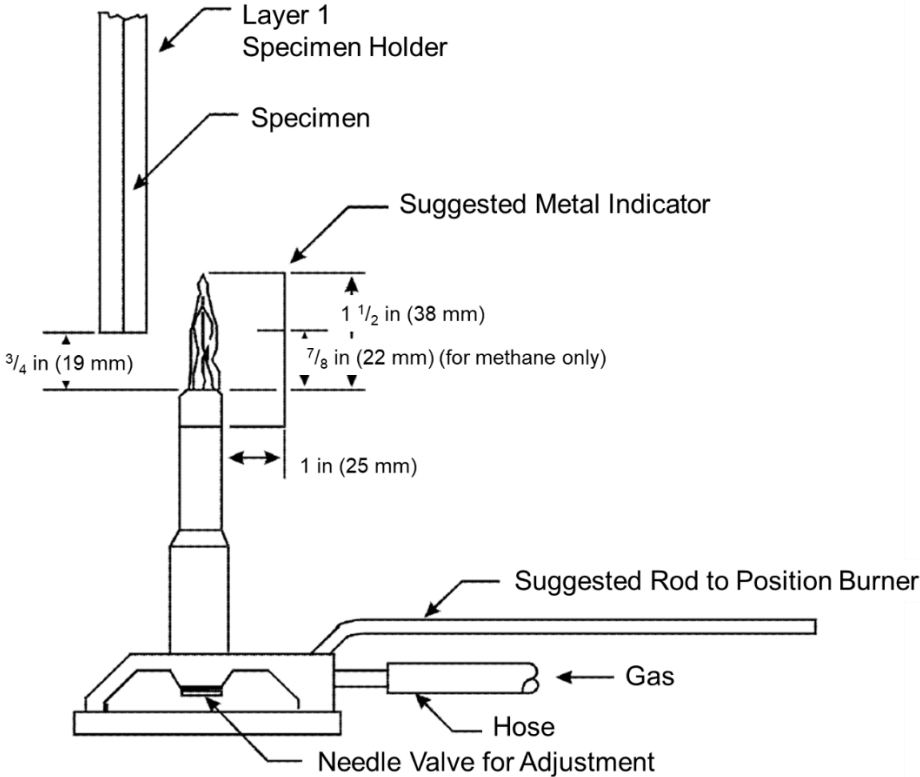
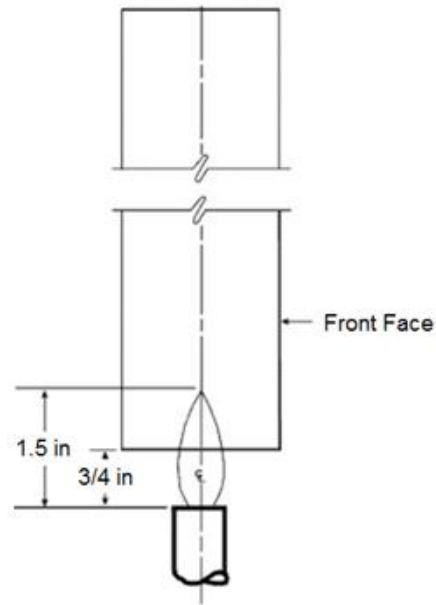
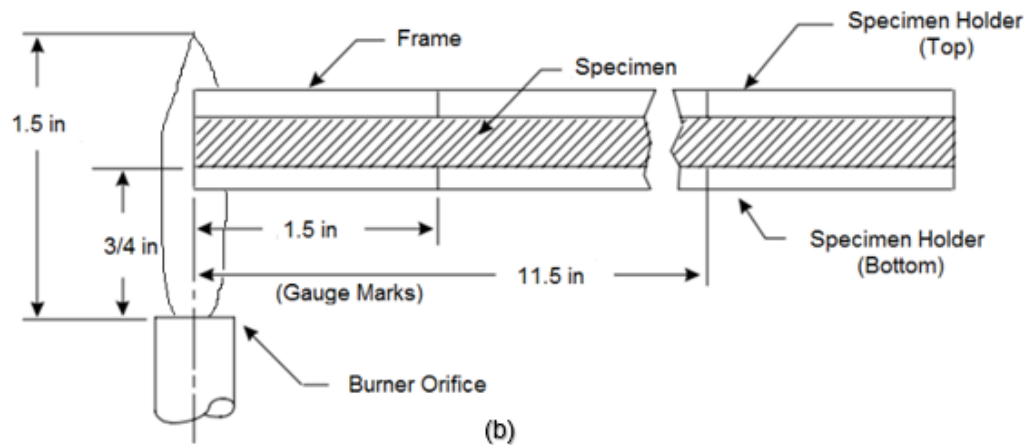


Figure 3.2 Burner plumbing and burner flame height indicator (Reprinted from [19]).



(a)



(b)

Figure 3.3 Schematic of specimen positioning with respect to the flame (a) for vertical fire tests and (b) horizontal fire tests (Adapted from [19]).

3.1.1. Vertical Bunsen Burner Fire Tests

The fire exposure durations adopted for the vertical burning tests on mechanically-failed graphite-epoxy UNC0, SBS, and IPS specimens were 12, 36, and

60 s. These times were based on low exposure (12 s) and high exposure (60 s) durations specified in the FAA Bunsen burner test protocols [19]. An intermediate test duration (36 s) was added to get a center point. To ensure the reproducibility of the results, a minimum of three replicates was used for all burning tests. Figure 3.4 shows a 21-ply cross-ply Cytec Cycom 5215 T40-800 graphite-epoxy UNC0 specimen during a vertical test using a Bunsen burner.



Figure 3.4 Picture of a 21-ply cross-ply Cytec Cycom 5215 T40-800 graphite-epoxy UNC0 specimen during vertical burning test using a Bunsen burner.

The thinner 16-ply IPS specimens subjected to 12, 36, and 60 s vertical fire tests experienced extreme thermal damage to individual graphite fibers, along with nearly complete matrix decomposition. This is likely due to the large free surface areas (*i.e.*, combustible area) that provided the opportunity for increased air flow (*i.e.*, oxygen supply) during the burning of this type of specimen. As a consequence, a

fourth set of vertical fire tests was performed on IPS specimens using a shortened fire duration of 6 s.

3.1.2. Horizontal Bunsen Burner Fire Tests

The FAA fire testing protocol [19] for horizontally-oriented specimens requires only one exposure time (typically 15 s). In this work, horizontal fire testing was performed on mechanically-failed graphite-epoxy UNC0, SBS, and IPS specimens for durations of 15, 45, and 75 s. These durations allowed an increment in fire exposure times similar to the vertical burning tests. For both vertical and horizontal tests, the intermediate and long exposure times were three and five times longer than the low exposure time defined by the FAA. Again, to ensure the reproducibility of the results, a minimum of three replicates was used for all horizontal burning tests. Figure 3.5 shows a 21-ply cross-ply Cytec Cycom 5215 T40-800 graphite-epoxy UNC0 specimen during a horizontal test using a Bunsen burner.



Figure 3.5 Picture of a 21-ply cross-ply Cytec Cycom 5215 T40-800 graphite-epoxy UNC0 specimen during horizontal burning test using a Bunsen burner.

3.2. Fire Application Using Cone Calorimeter

The cone calorimeter (Figure 3.6; reprinted with permission from [20]) is an instrument used for small-scale fire testing. Cone calorimetry can be used to determine many fire reaction properties for a bench-scale coupon in only a single test. These properties include the ignition time, peak and average heat release rate, time of sustained flaming, mass loss, smoke density, and the yield of soot, carbon monoxide (CO), carbon dioxide (CO₂), and other combustion gases formed during the burning process [3]. The cone calorimeter is based on the oxygen-depletion calorimetry technique that allows the measurement of the heat release rate by measuring the amount of oxygen consumed by the fire during the test [3, 9]. This is possible since the heat release per unit of oxygen consumed is constant [21].

The cone calorimeter is widely used in flammability tests since it provides similar burning conditions to a real (direct) fire test. In addition, cone calorimetry permits a wide range of heat fluxes (*e.g.*, 0-100 kW/m²) and can be used to *i*) predict the fire performance of a material in a large-scale fire test; *ii*) compare the fire reaction properties of different materials; *iii*) check whether or not a material meets the fire requirements necessary for a certain application; and *iv*) produce data to validate fire models [3].

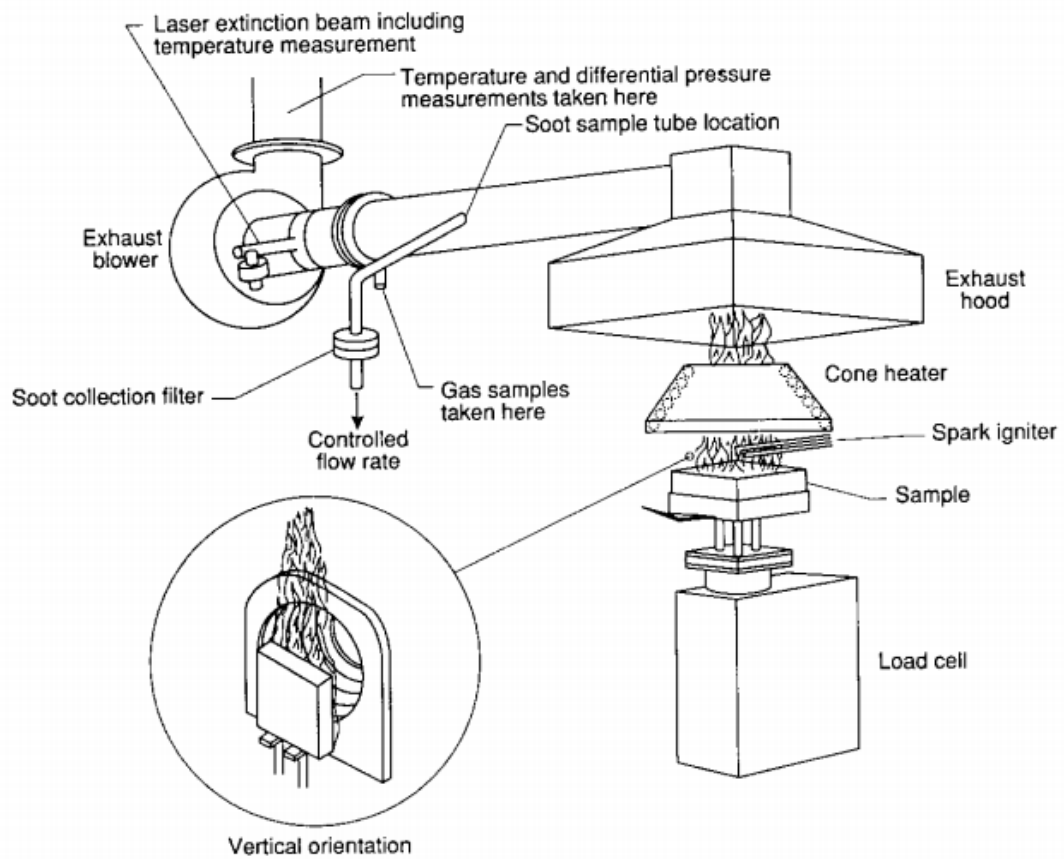


Figure 3.6 A schematic view of a cone calorimeter (Reprinted with permission from [20]).

4. TEST MATRIX

SEM was used to identify the fracture characteristics of specimens with three different failure modes (UNC0, SBS, and IPS). After identifying the features relevant to each failure mode, a series of vertical and horizontal fire tests were performed on UNC0, SBS, and IPS specimens. Consistent with the FAA Bunsen burner test protocols [19], three replicates were used for each test. Table 4.1 summarizes the exposure durations and the number of specimens tested for each failure mode for both the vertical and horizontal burning configurations. These tests were primarily performed to assess the effect of different fire exposure durations, specimen lay-up and failure surface morphology, and specimen orientation during testing on thermal damage development and char formation.

After burning, SEM was again used to characterize the fire damage induced in the UNC0, SBS, and IPS specimens for each burning configuration and fire exposure duration. The degree of char formation and thermal damage was compared for the different fire exposure durations and burning configurations to assess the influence of specimen geometry and fracture free surface area on the extent of the fire-induced damage.

Table 4.1 Summary of Mechanically-failed Specimens Subjected to Fire Testing.

Mechanically-failed Specimens Subjected to Fire Testing				
Burning Configuration	Fire Exposure Durations	UNC0	SBS	IPS
Vertical Burning	6 s	N/A	N/A	3
	12 s	3	3	3
	36 s	3	3	3
	60 s	3	3	3
Horizontal Burning	15 s	3	3	3
	45 s	3	3	3
	75 s	3	3	3

5. ANALYSIS OF MECHANICALLY-FAILED CYTEC CYCOM 5215 T40-800 GRAPHITE-EPOXY SPECIMENS SUBJECTED TO FIRE

The vertical and horizontal fire tests on mechanically-failed 21-ply UNC0, 45-ply SBS, and 16-ply IPS Cytec Cycom 5215 T40-800 graphite-epoxy specimens were all performed in accordance with the FAA Bunsen burner protocols. The fire damage on the fracture surface of the burned specimens was then investigated using a scanning electron microscope. For this purpose, the Tescan FERA-3-FIB-SEM was used to perform microscopy on vertically and horizontally burned UNC0, SBS, and IPS specimens. Due to the conductive nature of the residual char formed on the burned fracture surfaces, as well as the presence of naturally conductive graphite fibers, no sputter-coating was used. A conductive carbon tape was secured on the lateral surfaces of the specimens to reduce specimen charging and improve the quality of SEM images. All the SEM images presented in this section were taken at a voltage of 5 kV, a beam intensity of 8, and a working distance (WD) of 9 mm (unless otherwise stated).

5.1. Enclosed Vertical Fire Testing of Cytec Cycom 5215 T40-800 Graphite-epoxy Specimens

5.1.1. UNC0 Specimens

Fire tests on vertically-oriented 21-ply cross-ply Cytec Cycom 5215 T40-800 graphite-epoxy UNC0 specimens (lay-up: [90/0/90]₇) were performed for durations of 12, 36, and 60 s. Three repeat vertical fire tests were considered for each fire exposure duration. During the vertical tests on the UNC0 specimens, only the through-thickness

lateral specimen edges (sides) continued to burn after extinguishing the burner flame. The fracture surface, which was immersed in the source flame, extinguished a few seconds after the flame was stopped. This is likely due to the compact fracture surface area (Table 2.1) which restricted the oxygen transfer to the interior of the specimen. In addition, the char deposited at the fracture surface formed a thermal barrier that mitigated the spread of flame to the interior of the specimens [8]. For all three fire exposure durations, the fire damage on the UNCO specimens involved extensive pockets of matrix decomposition, soot deposits, char formation, and fire-induced delamination. The severity of the damage increased with increasing fire exposure duration.

Melt dripping of the epoxy matrix was observed during the 12 s fire tests. This tar-like substance (melt dripping) induced fire “sparkles” during specimen burning and leaked onto the tip of the Bunsen burner after the tests (Figure 5.1). The melt dripping of a given polymer strongly depends on its glass transition temperature, and the original polymer melt viscosity and degradation [22]. Unlike matrix decomposition which involves polymer bond breakage, during melt dripping a solid-viscous liquid phase change takes place inside the material due to high temperature exposure [22]. The relative degree and extent of the melt dripping was undoubtedly affected by the vertical specimen orientation during fire testing (*i.e.*, specimens were held upside down into the flame). In essence, any epoxy-based melt dripping would tend to accumulate on the broken carbon filament ends extending from the fracture surface; this arguably contributed to increased char deposits at and near these surfaces.

Recessed broken fibers were somewhat less prone to large-scale char deposition. Based upon both visual inspection and SEM imaging, char and soot were clearly visible on the extended fractured fiber ends and at the fracture surface. In general, fire damage was more severe at and near the fracture surface compared to the lateral edges (sides) and outer mold line (OML) and inner mold line (IML) planar surfaces of the composites. In addition, the severity of char and soot deposition was more pronounced around the perimeter of the fracture surface (*i.e.*, where the airflow and oxygen availability were ostensibly greater). In contrast, the region of the fracture surface in close proximity to the laminate mid-plane and specimen centerline tended to display relatively little char formation on the broken fiber ends, suggesting that any char formed due to matrix decomposition or melt dripping was burned off during direct flame exposure.



Figure 5.1 Fire sparkles during the 12 s vertical burn test on a 21-ply cross-ply Cytec Cycom 5215 T40-800 graphite-epoxy UNC0 specimen.

The fire damage (*i.e.*, extensive fire matrix decomposition, fire-induced delamination, and residual thickness increase) on specimens exposed to the 36 s and 60 s fire tests was more widespread and severe than that for the 12 s exposure. For specimens burned for the 36 and 60 s exposure durations, the damage extended throughout the total length of the specimens and fire-induced delamination occurred. The smoke released during the burning of the specimens was more intense as the fire exposure duration increased. The through-thickness delamination induced by the fire was more severe at the specimen outer plies. In addition, discrete matrix cracks formed parallel to the fibers in the outer 90-degree plies of the specimens. Figure 5.2 shows typical macro-scale pictures of an UNCO specimen (a) before and (b, c) after burning for 60 s. The fire damage includes char and soot deposition on the lateral edges and planar surfaces of the specimen, discrete matrix cracking, and ply-delamination.

In addition, the time for UNCO specimens to self-extinguish after the burner flame was stopped was highly dependent on the fire exposure duration. UNCO specimens burned for short durations (12 s) took more time to self-extinguish compared to specimens burned for longer fire durations (*i.e.*, 36 and 60 s). This makes sense since the degree of epoxy matrix decomposition and consumption for specimens with longer direct fire exposure was greater than that for specimens burned for less time. Moreover, the increased char layers formed in specimens with longer fire exposure likely impeded further burning once the direct flame was discontinued [3, 8].

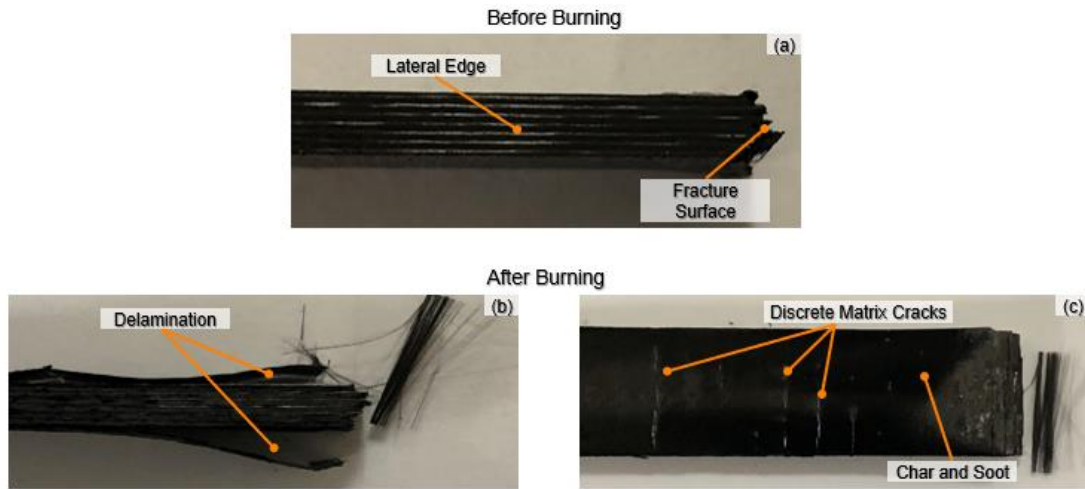


Figure 5.2 Pictures of a 21-ply cross-ply Cytec Cycom 5215 T40-800 graphite-epoxy UNC0 specimen; (a) before and (b) and (c) after vertical burning for 60 s.

In general, char formation was more pronounced around the perimeter than at the mid-plane of the fractured surfaces. Figure 5.3 shows typical SEM images of the char and soot that were deposited around the *perimeter* of the fracture surface of UNC0 specimens burned for (a) 12 s, (b) 36 s, and (c) 60 s. The figures identify char and soot deposition on the fractured fibers, pockets of matrix decomposition, and recessed fibers. Char was present on the broken fiber ends for all three fire exposure durations and was more pronounced for fibers along the perimeter edges that did not self-extinguish once the applied flame was removed. For all three fire exposure durations, the overall char formed on the fracture surface of the specimens increased slightly with increasing the fire duration. The residual char on the extended broken fibers had a fuzzy (cotton-candy-like) appearance and formed uniformly around the circumference of each fiber, with noticeably more char accumulation at the fractured filament ends. Figure 5.4 shows high magnification SEM images of char formation

around single fibers located on the perimeter of the fracture surface of UNCO specimens burned for (a) 12 s, (b) 36 s, and (c) 60 s.

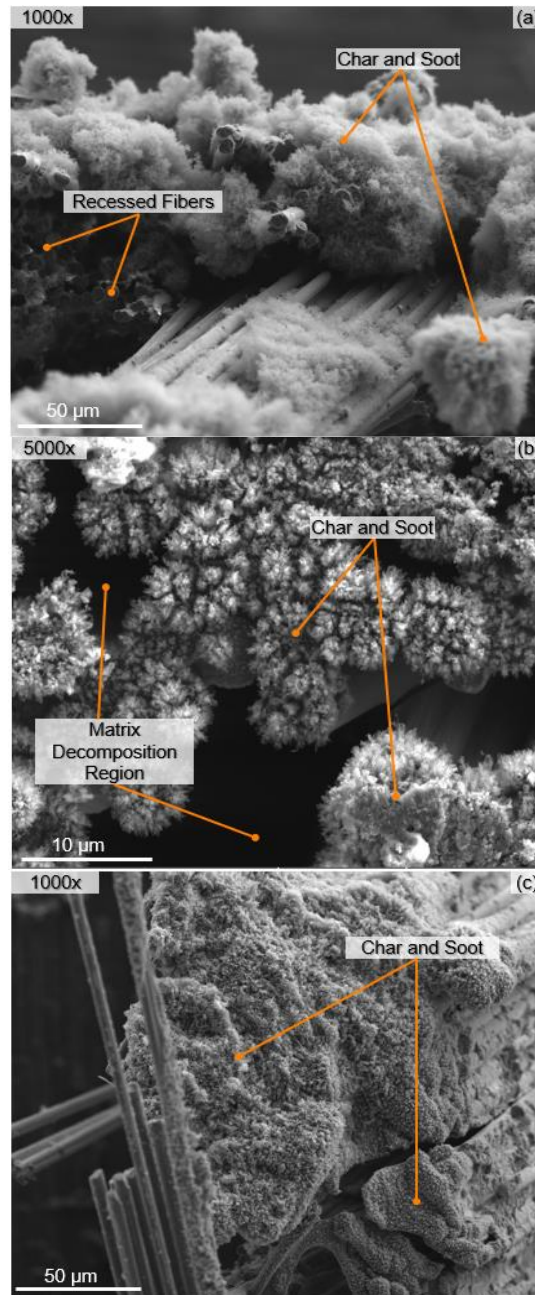


Figure 5.3 SEM images showing char and soot deposition around the perimeter of the fracture surface of 21-ply cross-ply Cytec Cycom 5215 T40-800 graphite-epoxy UNCO specimens burned vertically for (a) 12, (b) 36, and (c) 60 s.

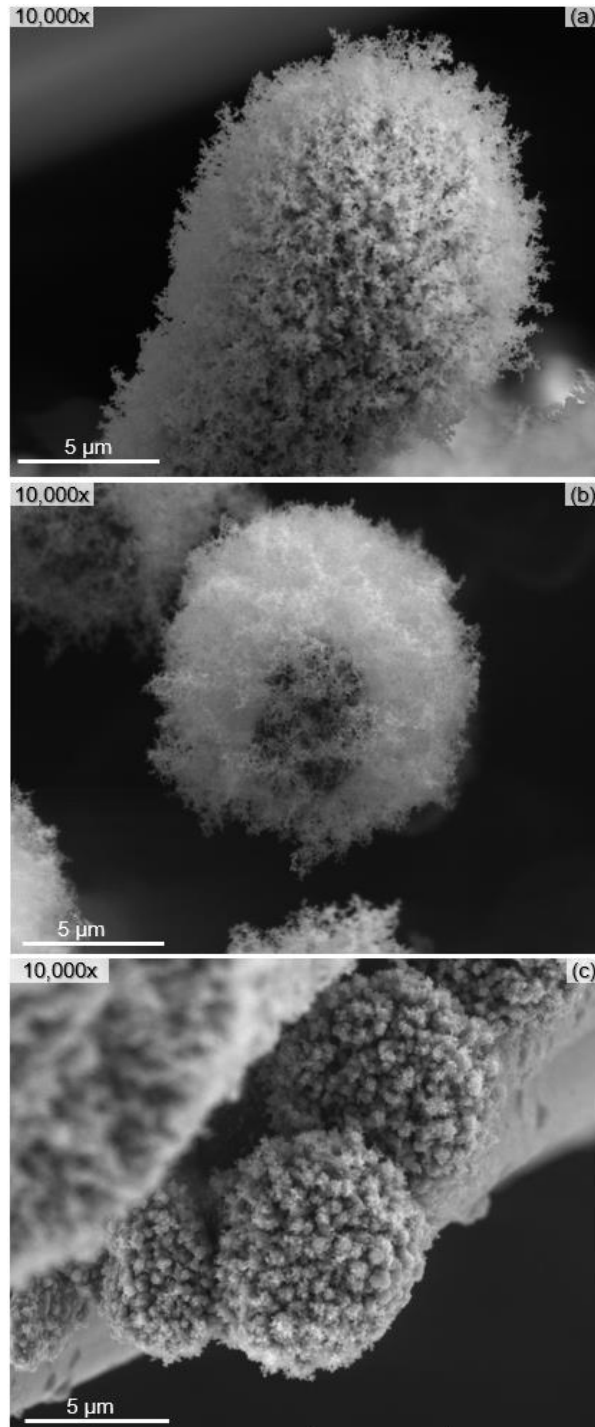


Figure 5.4 SEM images showing the fuzzy (cotton-candy-like) appearance of char formed around single fibers in 21-ply cross-ply Cytec Cycom 5215 T40-800 graphite-epoxy UNC0 specimens burned vertically for (a) 12, (b) 36, and (c) 60 s.

As mentioned previously, the residual char distribution was not uniformly distributed over the composite fracture surface. Little to no char was formed on broken fibers that were visibly *recessed* inside the specimens, which made it straightforward to identify key fracture characteristics of failed fibers even after fire exposure; this held true for all three fire exposure durations. For cross-ply laminates loaded in compression, fibers in the 0° plies typically fail due to buckling instabilities (*i.e.*, bending). A portion of a typical failed fiber fracture surface will have a rough appearance consistent with tensile failure. The remainder of the fiber cross-section will display “chop” marks that demarcate the transition from tensile to compressive failure. The appearance of chop marks can be used to define the location and orientation of the fiber neutral axis. Such features were still clearly visible for many recessed fibers in the burned UNCO specimens. Figure 5.5 compares the fiber fracture characteristics of (a) an UNCO specimen before burning, with those for slightly recessed fibers in UNCO specimens after burning for (b) 12, (c) 36, and (d) 60 s. In each burned specimen, indications of recessed fiber flexural failures were clearly visible even though such features became more difficult to see on extended broken fibers due to increased char formation.

In addition, fractured translaminar compression specimens may contain multiple thin “terraces” of failed and micro-buckled filaments [23]. Essentially, local material instabilities can give rise to kink bands consisting of terraces of short fractured fibers of approximately the same length. The kink band thickness is inversely proportional to the matrix modulus and is typically on the order of multiple

fiber diameters. Figure 5.6 (adapted with permission from [23]) shows a micrographic image of micro-buckling terraces at the fracture surface of a carbon fiber-reinforced polymer (CFRP) composite specimen failed in compression. Similar terraces of micro-buckled fibers were also observed in SEM images of the fracture surface of UNCO specimens vertically burned for 60 s (*cf.*, Figure 5.7). Even after extreme fire exposure, kink bands, micro-buckled fibers and their fracture surfaces were clearly identifiable. Given the loose arrangement of terrace-like structures, it may be possible to dislodge severely burned layers to expose relatively unaffected interior surfaces.

These results suggest that it may be possible to machine away (or otherwise dislodge) heavily charred regions of burned aerospace composite structures to reveal underlying (unburned) failure surfaces that can be used in post-crash forensic analyses. In addition to cotton-candy-like char deposits on broken fiber ends (Figure 5.4), a number of extended fibers appeared covered with solidified remnants of melt dripping (or its by-products) that had a cauliflower-like appearance. Figure 5.8 shows two SEM images of increasing magnification from an UNCO graphite-epoxy specimen burned for 36 s that clearly show the enveloped fiber ends, along with some evidence of char and soot residues. As shown in Figure 5.8, these cauliflower-like melt drip deposits had a solid viscous appearance that contrasts with the more fuzz-like char appearing elsewhere in the cross-section (Figure 5.4). Both types of deposits, however, completely mask the salient aspects of fiber fracture surface morphology necessary to identify the operative mechanical failure modes. Any chemical or physical attempts at char removal aimed at facilitating post-crash forensic analysis in

composites subjected to fire would likely have to account for key differences in the chemistry and morphology of the carbonaceous fire by-products deposited on the broken filament ends.

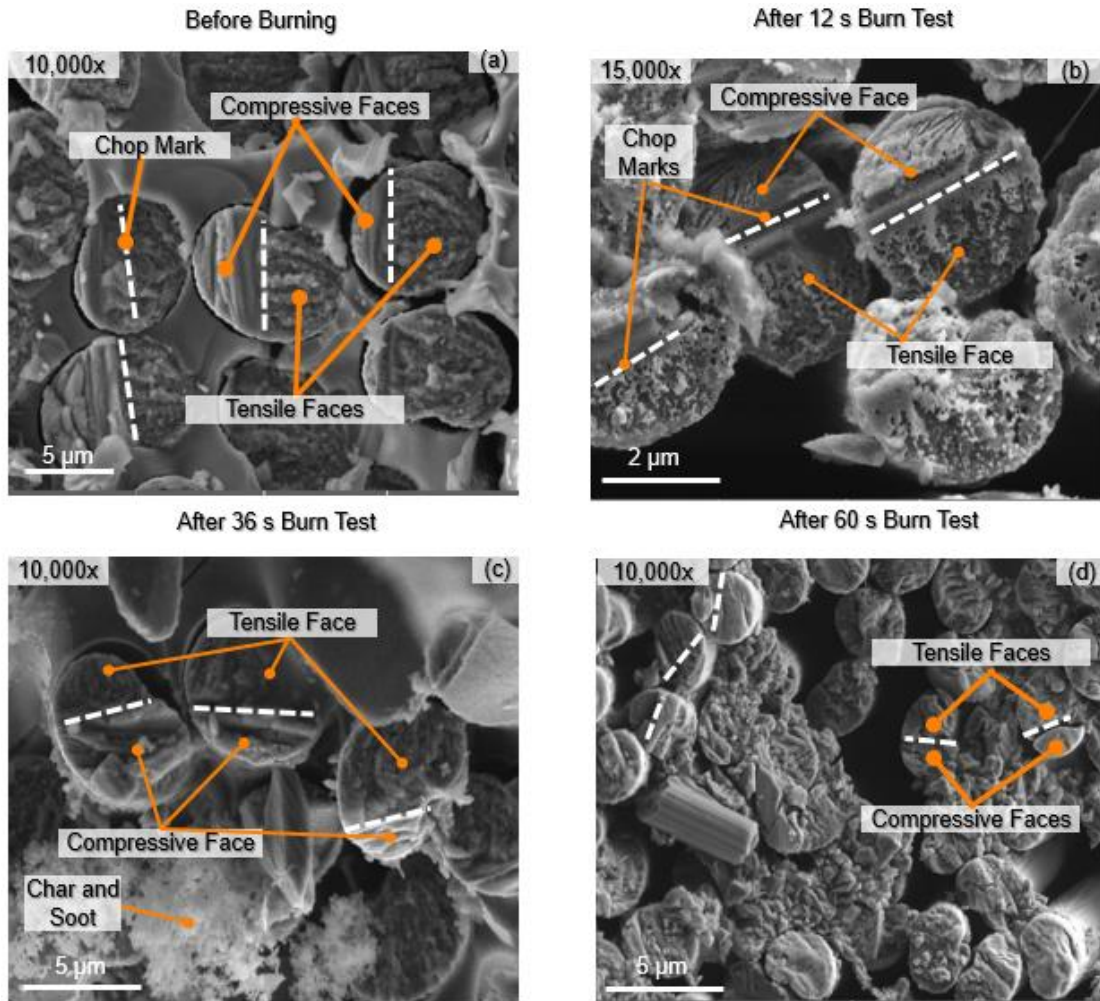


Figure 5.5 Fracture characteristics on (a) a 21-ply cross-ply Cytec Cycom 5215 T40-800 graphite-epoxy UNC0 specimen before burning, and on recessed fibers on specimens of the same failure modes after vertical burning for (b) 12, (c) 36, and (d) 60 s.

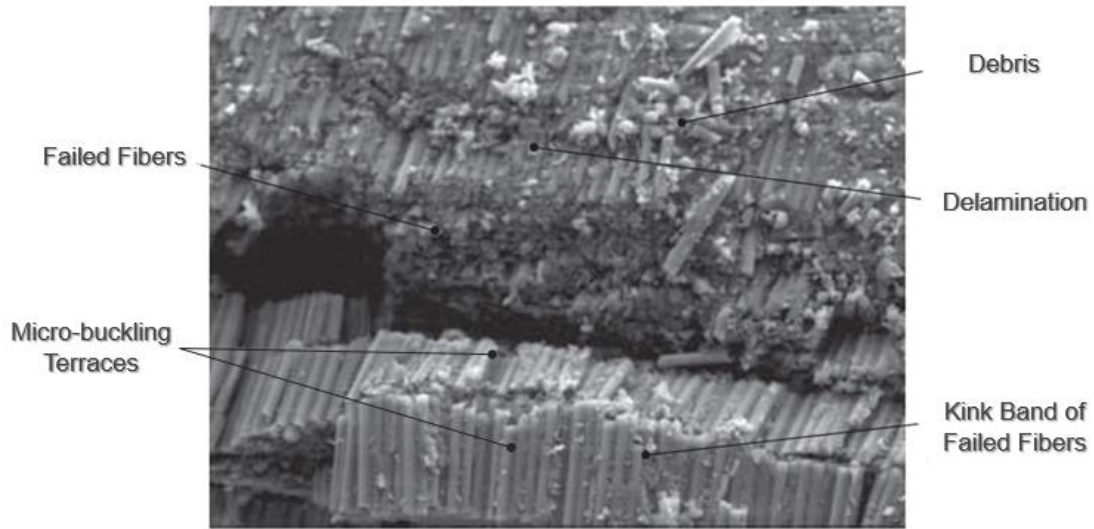


Figure 5.6 Micro-buckling terraces on compression failed CFRP specimen (x700) (Adapted with permission from [23]).

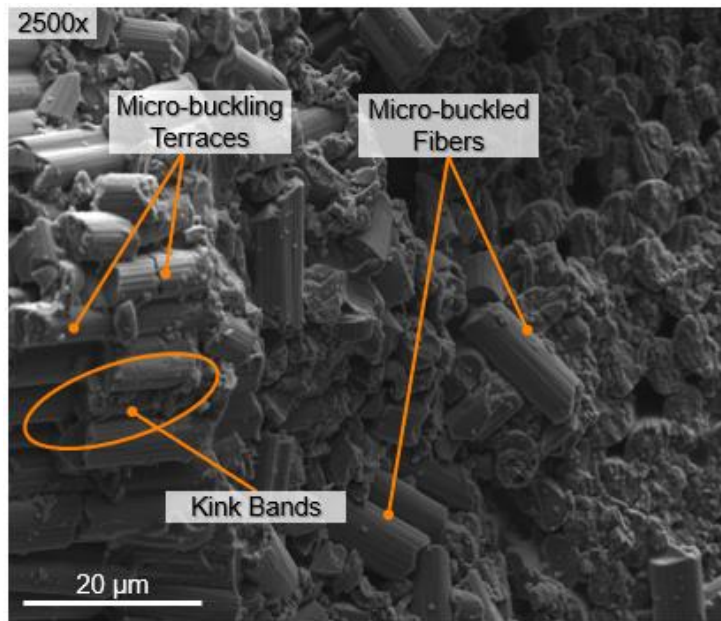


Figure 5.7 SEM image showing micro-buckled fibers in a 21-ply cross-ply Cytec Cycom 5215 T40-800 graphite-epoxy UNC0 specimen burned vertically for 60 s.

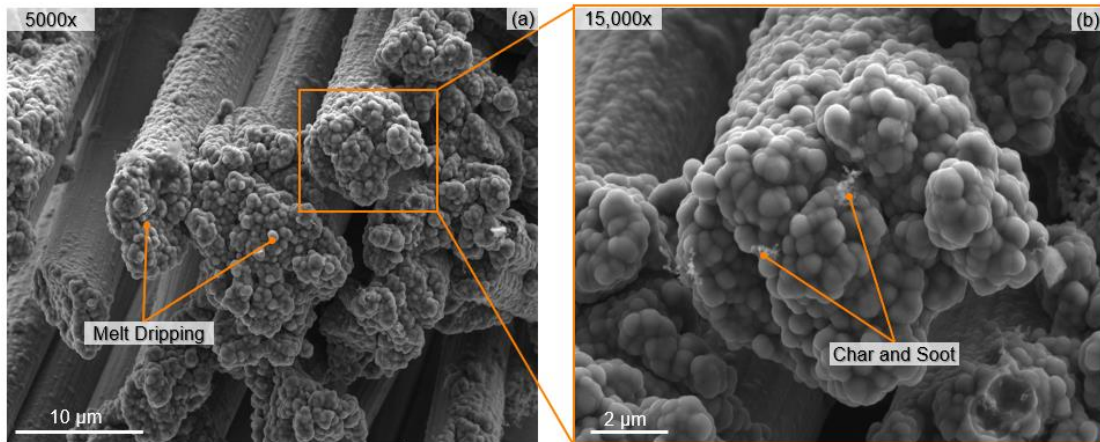


Figure 5.8 (a) Melt dripping on fracture fibers ends of a 21-ply cross-ply Cytec Cycom 5215 T40-800 graphite-epoxy UNC0 specimen burned vertically for 36 s (b) a magnified view of filaments covered with melt dripping.

UNC0 graphite-epoxy specimens burned for extended durations also experienced fire-induced delamination, ply-splitting, and matrix-cracking. Figures 5.9a, b show delamination between plies and ply-splitting in an UNC0 specimen after a 60 s burn test. Figure 5.10 shows matrix cracking in the same specimen. Delamination, ply-splitting, and matrix cracking result from large internal local pressures due to the formation of combustion gases, smoke, and vaporized moisture that try to escape to the exterior [3, 10]. Such damage can also arise from thermally induced-strain and temperature gradients in a laminate [3, 10], which can be exacerbated by large differences in local ply orientations such as those occurring in cross-ply UNC0 specimens. In addition, temperature-induced thermal softening of the matrix can result in significant reductions in composite interlaminar fracture toughness and contribute to increased matrix cracking and delamination [10].

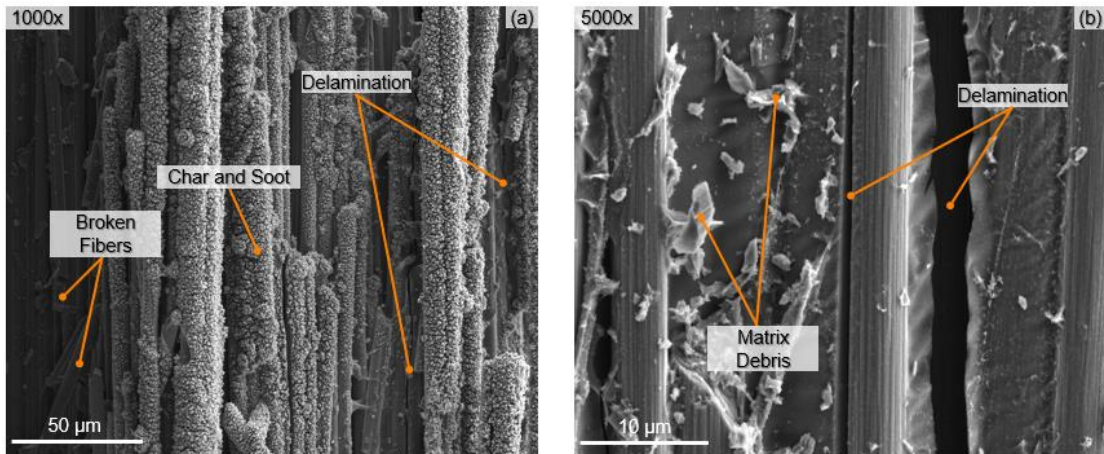


Figure 5.9 Delamination in a 21-ply cross-ply Cytec Cycom 5215 T40-800 graphite-epoxy UNC0 specimen burned vertically for 60 s.

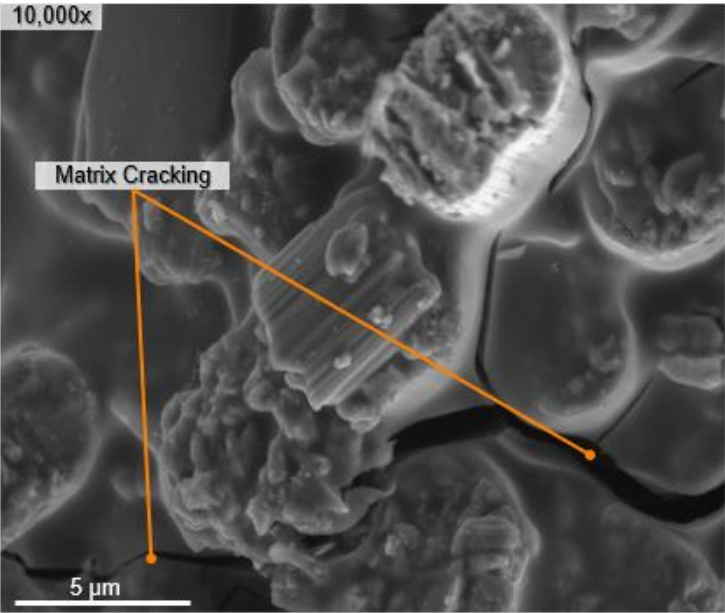


Figure 5.10 Matrix cracking in a 21-ply cross-ply Cytec Cycom 5215 T40-800 graphite-epoxy UNC0 specimen burned vertically for 60 s.

5.1.2. SBS Specimens

Vertical fire tests were performed on 45-ply unidirectional Cytec Cycom 5215 T40-800 graphite-epoxy SBS specimens (lay-up: $[0]_{45}$) for durations of 12, 36, and 60 s to assess the effects of flame exposure time on char formation. Three repeats were performed for each fire exposure time. Fire damage (*i.e.*, extensive fire matrix decomposition, soot, char, and residual thickness increase) observed was more severe for specimens subjected to the flame for 36 and 60 s. The fire damage mechanisms generated in the vertical burning tests on the SBS specimens were similar to those in the UNCO specimens and extended throughout the length of the burned specimens. Again, the relatively thick SBS and UNCO specimens both display a more compact failure surface that inhibits oxygen flow to the interior of the specimens, resulting in more char formation around the perimeter of the cross-section. Char deposition at the SBS fracture surfaces also served as a thermal barrier that reduced fire damage penetration into the composite at the laminate interior; this is consistent with observations from the literature [3, 8]. Again, for all three fire exposure durations, the lateral specimen edges (sides) continued to burn after the flame was extinguished. Similar to UNCO specimens, SBS specimens exposed for 12 s took longer to self-extinguish than for 36 and 60 s fire tests. Figure 5.11 shows typical macro-scale pictures of an SBS specimen (a) before and (b) after fire exposure for 60 s. The fire damage included local delamination near the fracture surface, char formation and soot deposition on the lateral edges and outer ply surfaces, and a significant increase in the residual thickness of the burned specimen.

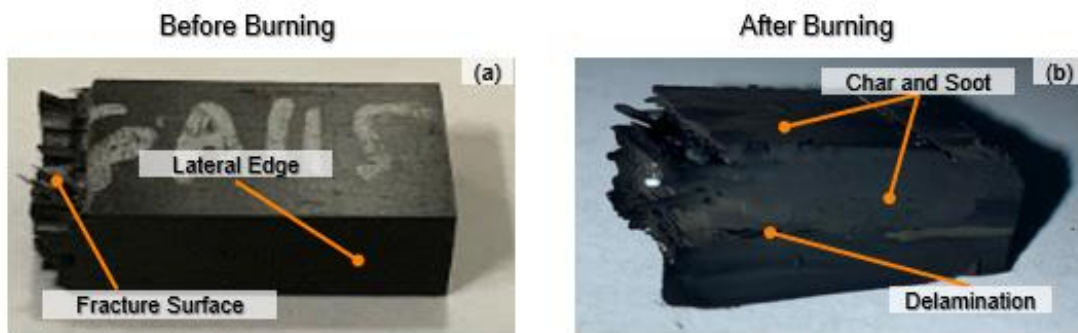


Figure 5.11 Picture of a 45-ply unidirectional Cytec Cycom 5215 T40-800 graphite-epoxy SBS specimen; (a) before and (b) after vertical burning for 60 s.

Mechanically-failed SBS specimens subjected to three-point bending will break into two distinct halves, as suggested by the single half shown in Figure 5.11 a. Occasionally, an individual half will longitudinally split (*i.e.*, completely delaminate) into two $\frac{1}{4}$ -specimens due to high inter-laminar stresses. Pairs of mating $\frac{1}{4}$ -specimens were clamped together and subjected to 12, 36, and 60 s fire exposure tests. After 12 s of fire exposure, the mating pieces remained separated. After 36 and 60 s of fire exposure, however, the mating pieces adhered together. Clearly, increased fire exposure led to some degree of interfacial bonding between initially separated layers. This could be due to various aspects of melt dripping and subsequent matrix decomposition, or the presence of tougheners, surfactants, plasticizers, flame retardants or other additives blended into the commercial Cycom 5215 epoxy prior to resin infusion and curing. The exact composition of most commercially-available thermosetting epoxies is proprietary and very difficult to determine. It is unclear whether the use of unmodified (neat) epoxy would lead to the same adhesion between

separated layers upon reheating; this issue remains to be fully explored. Nonetheless, the local chemistry at these interfaces for Cycom 5215 epoxy may be similar to that for the melt dripping observed throughout these family of tests and may provide insight into char formation (and removal) on graphite/carbon fiber surfaces. The effect of melt dripping and/or similar phenomena may become increasingly pronounced for thicker specimens where the total volume of cured matrix is greater and incomplete decomposition/combustion of the matrix is increasingly likely.

Figures 5.12a, c show SEM micrographs taken from the perimeter of the fracture surface of vertically burned SBS graphite-epoxy specimens exposed to direct flame for 12, 36, and 60 s, respectively. Similar to the UNCO specimens (Figure 5.3), proportionally more char accumulated at and near extended broken fibers located around the perimeter of the cross-section where the airflow was greater; little char formed on extended fibers located near the laminate mid-plane. Specimens burned for only 12 s displayed apparent accumulations from melt dripping at the broken filament ends (Figure 5.12a) with very little soot and char deposits. The presence of melt dripping coupled with low amounts of char suggests relatively incomplete combustion/decomposition of the epoxy matrix occurred for the 12 s flame exposure, which no doubt was influenced by the relatively thick SBS specimen geometry. While not shown here, melt dripping was also observed along the lateral edges (sides) of the SBS specimens. Specimens burned for 36 and 60 s (Figures 5.12b, c, respectively) exhibited increasing amounts of extensive char formation on extended broken fibers, as well as appreciable soot deposition. Similar to results for UNCO specimens, the

char formed at and around the extended fiber ends exhibited a fuzzy (cotton-candy-like) appearance (Figure 5.13).

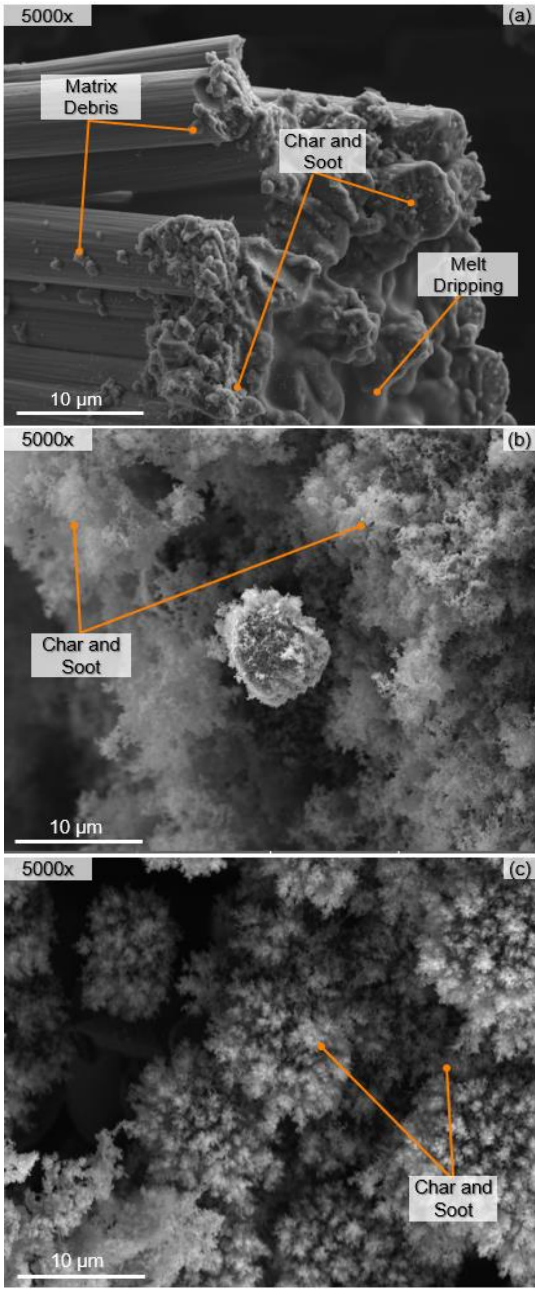


Figure 5.12 SEM images showing char and soot deposition on the fracture surface of 45-ply unidirectional Cytec Cycom 5215 T40-800 graphite-epoxy SBS specimens after vertical burning for (a) 12, (b) 36, and (c) 60 s.

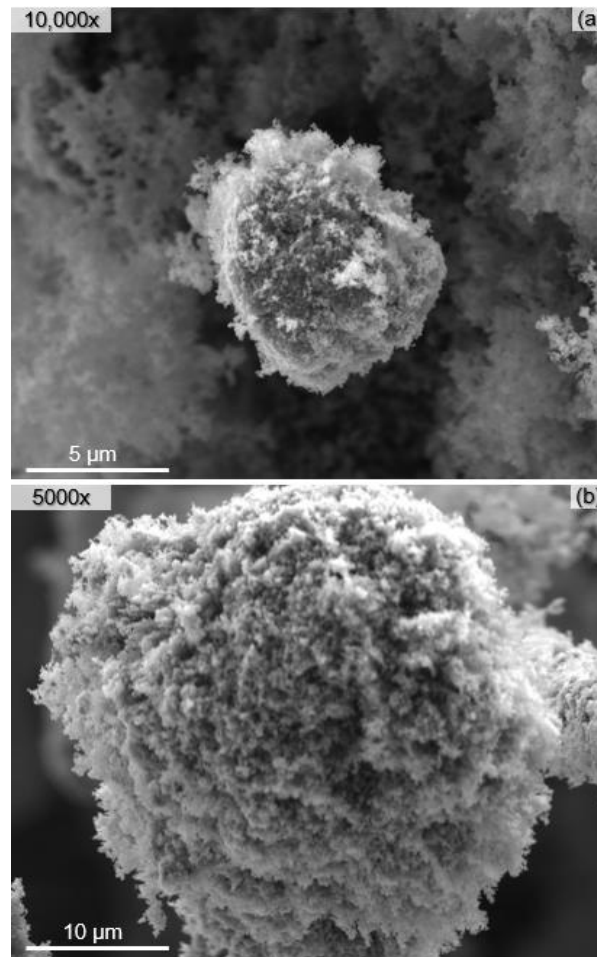


Figure 5.13 SEM images showing the fuzzy (cotton-candy-like) appearance of char formed around single fibers in 45-ply unidirectional Cytec Cycom 5215 T40-800 graphite-epoxy SBS specimens burned vertically for (a) 36, and (b) 60 s.

It is clear that *extended* fibers emanating from the mean fracture surface of failed UNCO and SBS specimens are prone to accumulation of melt dripping, char, soot, and other deposits that mask key aspects of fracture surface morphology. Hence, physical, chemical, and/or thermal strategies for char removal must be developed in order to perform forensic analysis of these original mechanical failure surfaces (without damaging or destroying the surfaces). A number of such approaches are

being explored by other researchers as a complementary part of this overarching effort. As mentioned previously, inspection of visible *recessed* broken fibers may permit the identification of operative mechanical fiber failure mechanisms. For example, Figure 5.14 contains SEM images of recessed fibers in an unburned SBS specimen, as well as for specimens burned for 12, 36, and 60 s. In each case, rough tensile failure surfaces and compressive chop marks were clearly visible on numerous *recessed* fibers; such features became increasingly obscured on *extended* filament ends as the fire duration was increased.

Similar to UNC0 specimens (Figure 5.6 adapted with permission from [23]), terraces of micro-buckled fibers formed in *compressive* regions of failed three-point bend SBS specimens. Figures 5.15a, b show SEM images of micro-buckled fibers in a SBS specimen before fire exposure. Figure 5.15c shows the same specimen after vertical burning for 60 s. After burning, parallel clusters of micro-buckled fibers indicative of compressive failure were still visible, albeit covered in char; some slant-like fiber fracture features also remained. In nearby regions of the specimen, micro-buckled fibers in terrace structures were completely covered with melt dripping (Figure 5.16). This suggests that removal of the outer terraces may be desirable to better identify operative mechanical failure mechanisms.

The vertical fire tests performed on UNC0 and SBS specimens suggest that a sequence of thermally activated processes contribute to char formation on broken graphite fibers that strongly depend on the flame duration, specimen geometry and lay-up, spatial location within a given cross-section, original fracture surface

morphology, local extension/recession of individual filaments, air-flow, oxygen availability, and other factors. A potential sequence of these events can be summarized as follows: Upon initial heating of the composite, melt dripping occurs that leads to thick gooey deposits on the extended filament ends emanating from the fracture surface (Figure 5.12a). As the fire exposure is increased, these deposits increasingly decompose and combust, leading to fuzzy or cotton-candy-like char deposits on the fiber ends (Figures 5.12b, c). As the flame duration is further increased, the char is completely decomposed/consumed, leaving bare fibers; this may explain a large number of exposed fibers at the laminate mid-planes after significant fire exposure. This sequence of events is not terribly dissimilar from processes used in ASTM standard matrix ignition tests [15] and efforts aimed at recycling carbon fibers from thermoset composites [16, 17]. Of course, large-scale fire exposure to bare graphite or carbon fibers has the potential to severely damage and decompose the fibers.

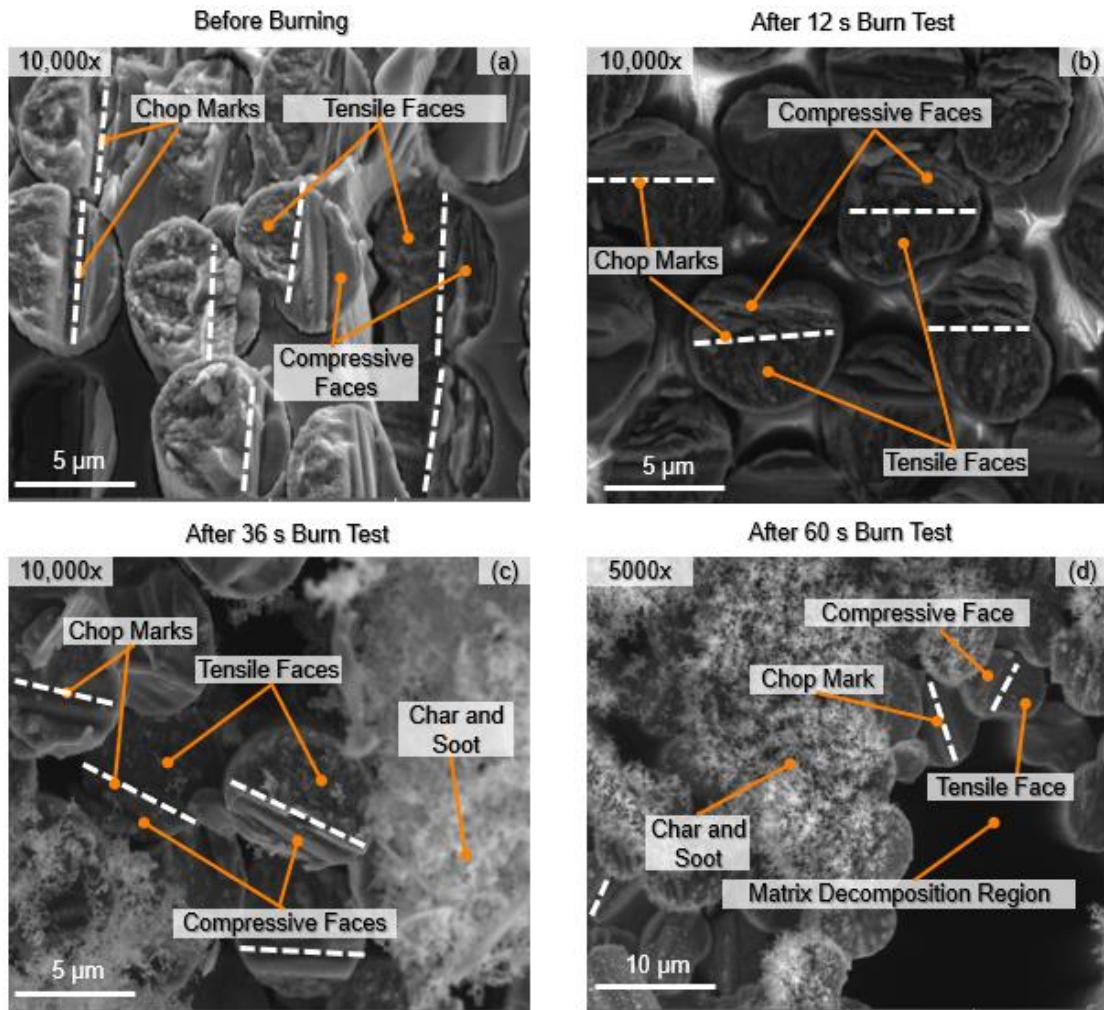


Figure 5.14 Fracture characteristics on (a) a 45-ply unidirectional SBS Cytec Cycom 5215 T40-800 graphite-epoxy specimen before burning, and on recessed fibers on specimens of the same failure modes after vertical burning for (b) 12, (c) 36, and (d) 60 s.

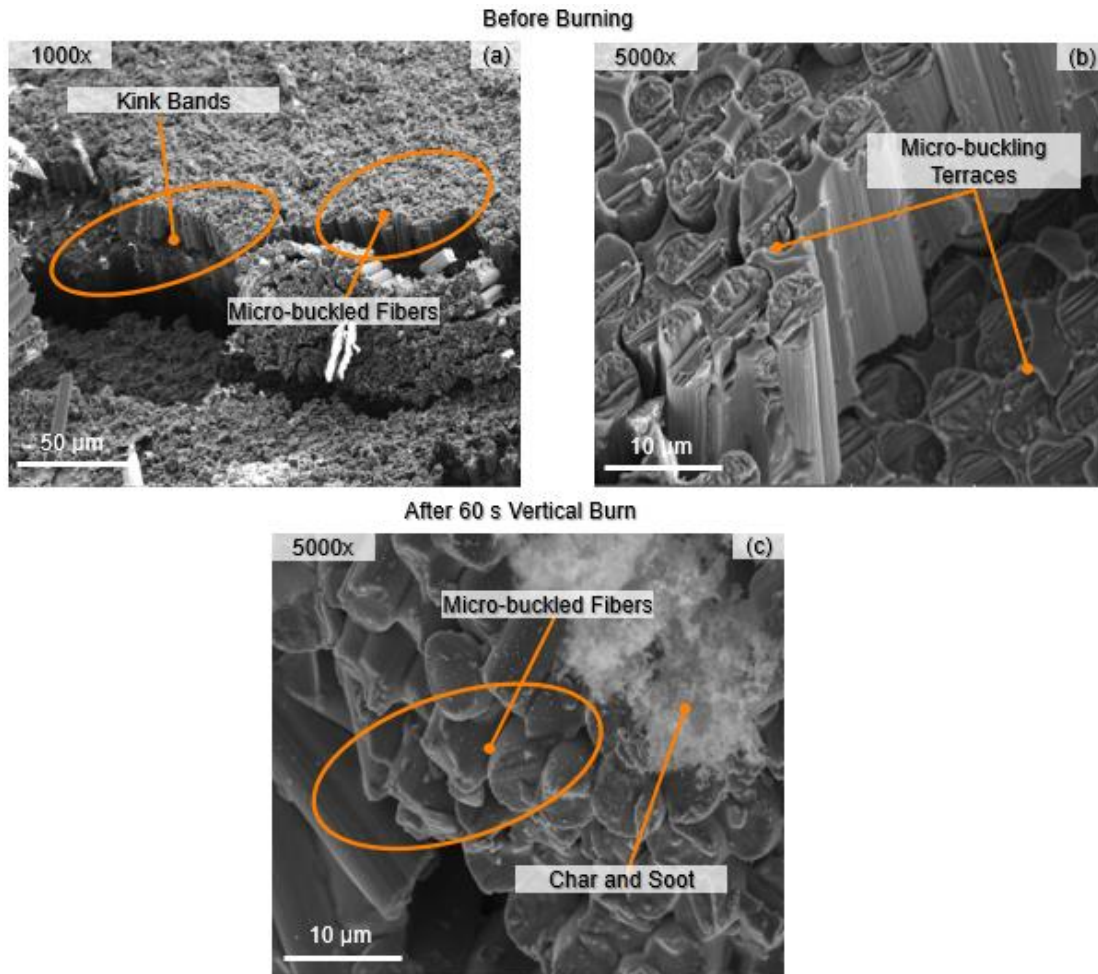


Figure 5.15 Micro-buckled fibers in Cytec Cycom 5215 T40-800 graphite-epoxy SBS specimens: (a) unburned specimen, (b) magnified view of the unburned specimen, and (c) specimen vertically burned for 60 s.

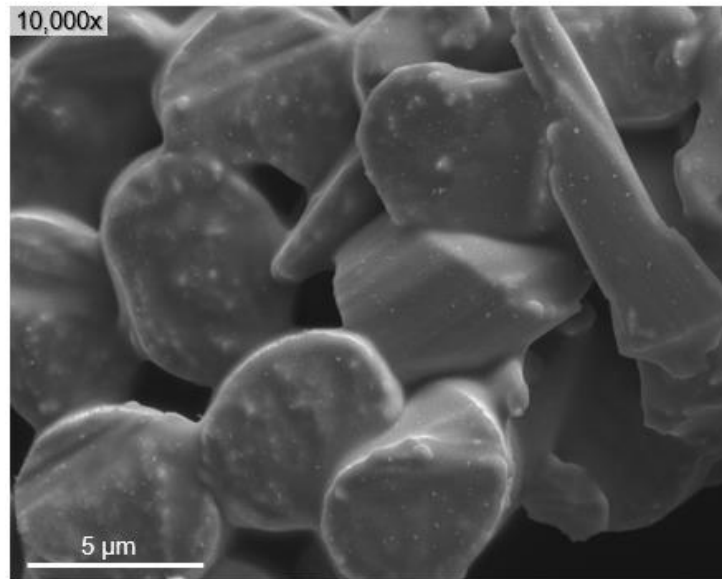


Figure 5.16 Micro-buckled fibers in Cytec Cycom 5215 T40-800 graphite-epoxy SBS specimens completely covered in melt dripping.

5.1.3. IPS Specimens

Vertical fire tests were performed on 16-ply Cytec Cycom 5215 T40-800 graphite-epoxy IPS specimens (lay-up: $[45/-45]_{4S}$) for durations of 6, 12, 36, and 60 s to assess the effect of fire exposure on char formation. Three repeats were performed for each exposure time. Unlike UNCO and SBS specimens that tend to fail within a more planar damage zone, individual IPS plies tend to fail along multiple offset planes that are oriented at $\pm 45^\circ$ to the axial loading direction (*i.e.*, perpendicular to the local ply orientation). In addition, failure involves extensive fiber tow splitting and delamination between plies. As a consequence, there is much more free surface (combustible) area created during failure of the angle-ply IPS specimens than for cross-ply UNCO and unidirectional SBS specimens, and the IPS damage distribution is far-more diffuse (see inset figure included in Table 2.1).

Due to their highly irregular fracture surface geometries, the IPS specimens were positioned above the Bunsen burner during fire tests such that the blue tip of the flame was at the same level as the fractured fibers at the longest lateral edge of the specimen, as shown in Figure 5.17 and location 1 in Figure 5.18a. Specimens subjected to fire exposures of 12, 36, and 60 s each experienced large-scale matrix decomposition and delamination that increased substantially with increasing fire exposure. For longer exposure times, almost complete matrix decomposition occurred over the majority of the specimens and fire-induced delamination spanned the entire length of the specimens. Virtually no char, soot, or epoxy was visible at the graphite filament ends located at the laminate midplane along the centerline of the composite that were exposed to direct flame (location 2 in Figure 5.18a); bundles of bare graphite fibers (with no evidence of cured epoxy matrix or char) remained at this location after burning. IPS specimens burned for 12, 36, and 60 s were largely destroyed during fire testing. These specimens displayed much higher degrees of matrix decomposition, significantly lower levels of residual char formation, and more fiber thermal damage than the UNCO and SBS specimens tested under similar conditions. The large free surface area present in failed IPS specimens resulted in enhanced oxygen flow throughout the specimens, more complete combustion of the organic matrix, and relatively little residual char formation. For these reasons, additional vertical tests of IPS specimens were performed with a *reduced fire exposure duration* of 6 s. In contrast to the UNCO and SBS specimens, which generated more char on exposed fiber ends with increasing fire exposure times, the

maximum char formed on extended fibers in IPS specimens occurred for a 6 s exposure time.



Figure 5.17 Positioning of the IPS specimen during vertical burn tests.

Figure 5.18 shows typical macro-scale pictures of an IPS specimen (a) before and (b, c) after fire exposure for 6 s. Char and soot were observed on the exposed filament ends, lateral specimen edges (sides), and on planar outer ply surfaces. Pre-existing mechanical delamination appeared to grow significantly after fire exposure. The locations 1 (longest lateral edge), 2 (laminate centerline), and 3 (shortest lateral edge) shown in Figure 5.18a define the approximate locations of SEM images taken of the failure surfaces. Figure 5.19 shows that IPS specimens burned for 6 s developed significant char on extended fibers at both lateral edges, as well as the laminate centerline.

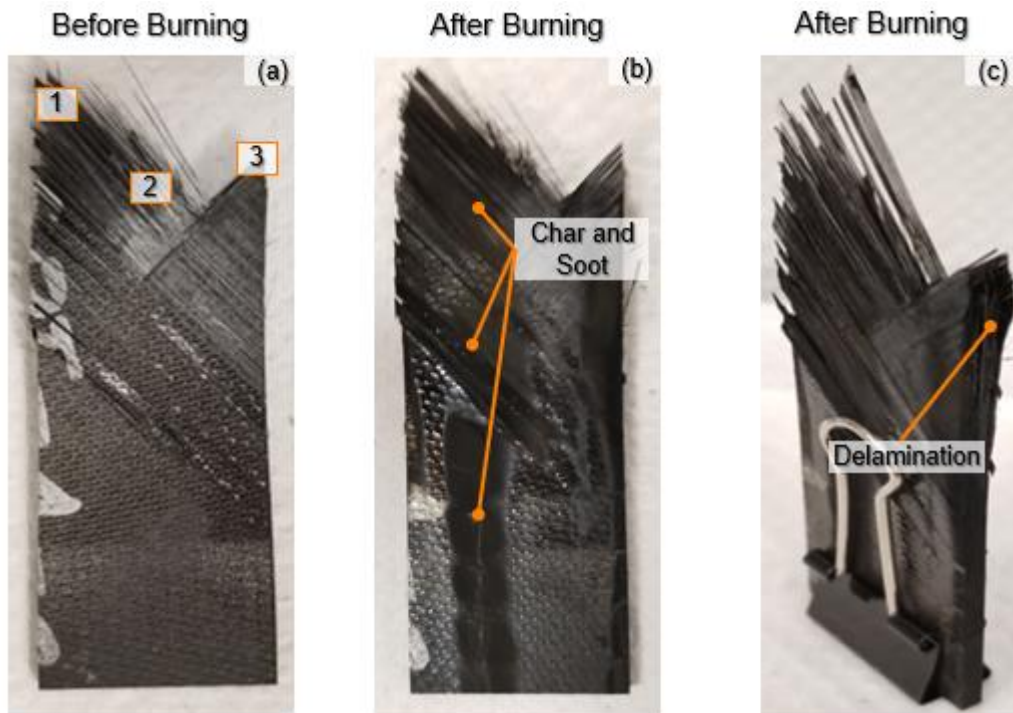


Figure 5.18 Pictures of a 16-ply Cytec Cycom 5215 T40-800 graphite-epoxy IPS specimen (a) before and (b) and (c) after vertical fire exposure for 6 s. In (a), locations 1, 2, and 3 denote the longest lateral edge, laminate centerline, and shortest lateral edge, respectively.

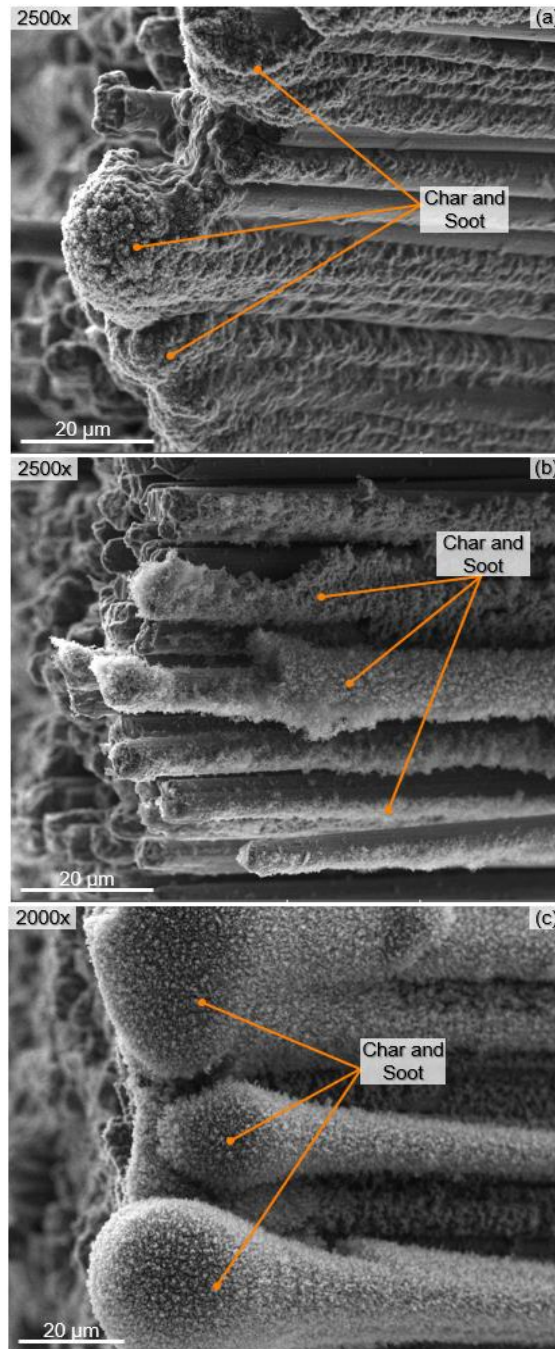


Figure 5.19 SEM micrographs showing char and soot deposition on fractured fibers located at (a) the longest lateral edge, (b) center and (c) shortest lateral edge of 16-ply Cytec Cycom 5215 T40-800 graphite-epoxy IPS specimens subjected to 6 s vertical burn test. These correspond to locations 1, 2, and 3, respectively, in Figure 5.18a.

For IPS specimens subjected to longer fire exposure times (*i.e.*, 12, 36, and 60 s), virtually no residual char formed on fibers located near the *longest lateral edge* (location 1 in Figure 5.18a) or at the specimen *centerline* (location 2 in Figure 5.18a). In contrast, significant char only formed on broken fiber ends located near the *shortest lateral edge* (location 3 in Figure 5.18a); this location was farther removed from the blue flame tip than the other points considered. Figures 5.20a–5.22a show SEM images of the fracture surface at the longest lateral edge for specimens burned for 12, 36, and 60 s, respectively. Similarly, Figures 5.20b–5.22b show SEM images of the increasing amounts of char and soot deposited on fibers at the shortest lateral edge for specimens burned for 12, 36, and 60 s, respectively. Since no significant char was present at the longest lateral edge for specimens, epoxy matrix cracks, angled fiber fractures, matrix debris, and micro-buckled fibers are all clearly visible in the images. These features are similar to typical fracture characteristics found in *unburned* IPS specimens. Any char that did form and then was subsequently burned off did not appear to significantly change the identifiable mechanical failure mechanisms. This trend did not hold true, however, for fibers located along the centerline of the IPS specimens. As an aside, the SEM images presented in Figures 5.20–5.22 were taken at different working distances (WDs) to accommodate for large variations in specimen geometries, as well as differences in the out-of-plane locations of individual clusters of fibers.

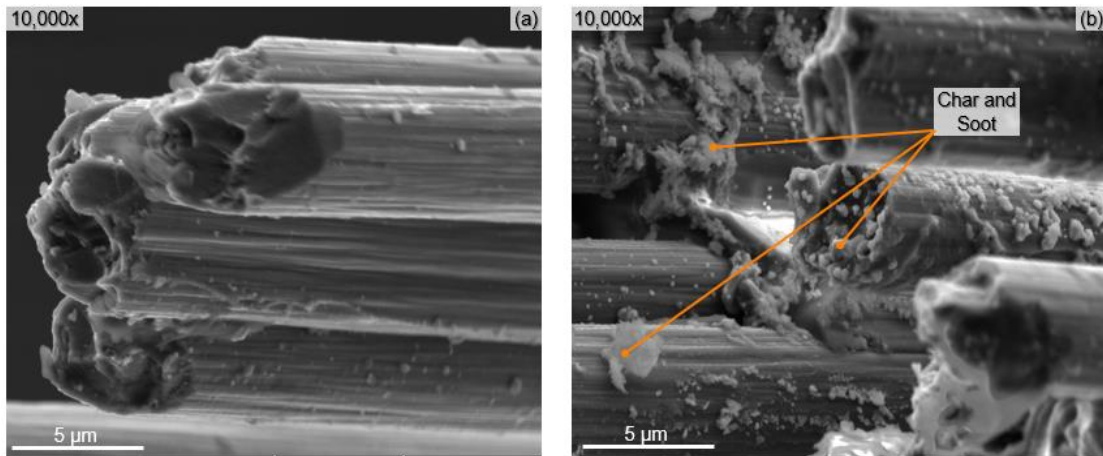


Figure 5.20 SEM images showing char formation on (a) the longest and (b) shortest lateral edges of 16-ply Cytec Cycom 5215 T40-800 graphite-epoxy IPS specimens burned vertically for 12 s both taken at a WD of 15 mm. These correspond to locations 1 and 3 in Figure 5.18a.

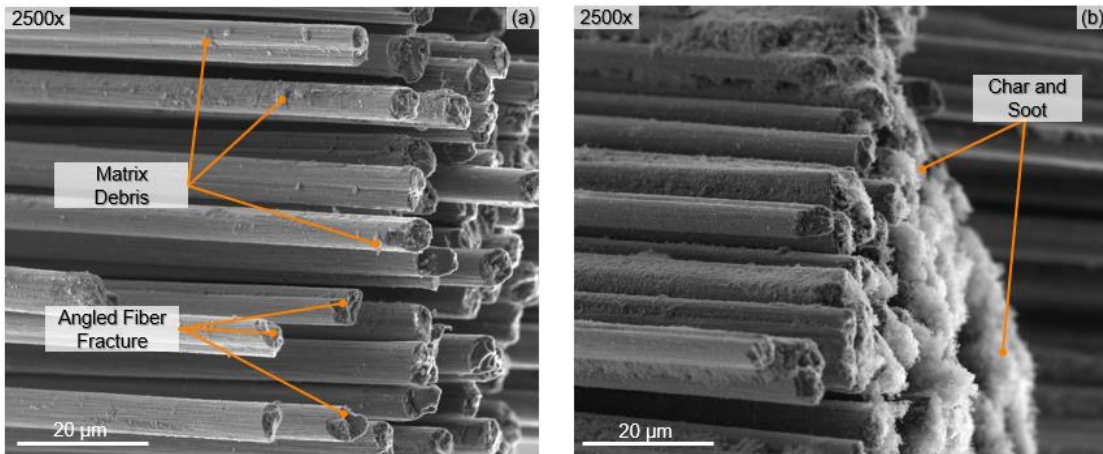


Figure 5.21 SEM images showing char formation on (a) the longest and (b) shortest lateral edges of 16-ply Cytec Cycom 5215 T40-800 graphite-epoxy IPS specimens burned vertically for 36 s taken at WDs of 9 and 11 mm, respectively. These correspond to locations 1 and 3 in Figure 5.18a.

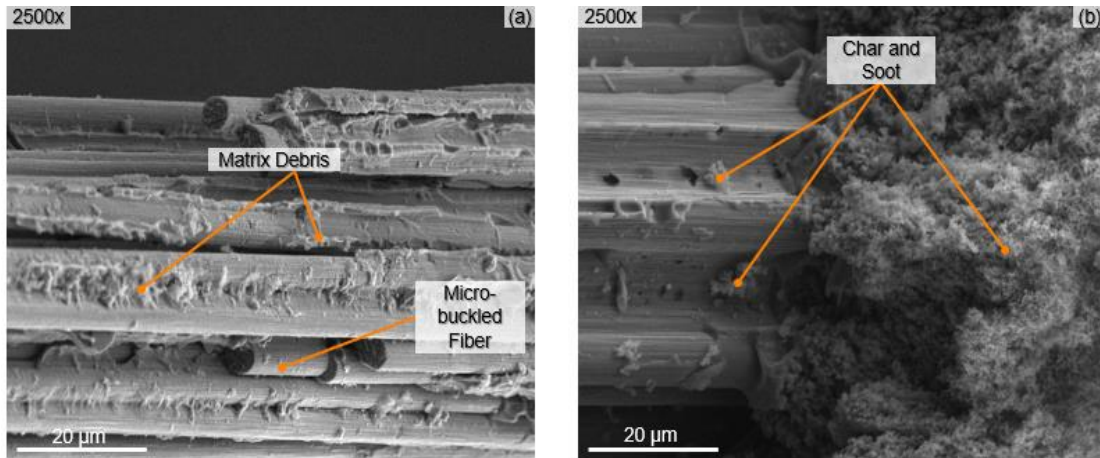


Figure 5.22 SEM images showing char formation on (a) the longest and (b) shortest lateral edges of 16-ply Cytec Cycom 5215 T40-800 graphite-epoxy IPS specimens burned vertically for 60 s taken at WDs of 12 and 25 mm, respectively. These correspond to locations 1 and 3 in Figure 5.18a.

Exposed graphite filaments located near the mid-plane of the fracture surface along the IPS specimen centerline (location 3 in Figure 5.18a) were severely altered when specimens were burned for 12, 36, and 60 s. The fibers thermal degradation was so severe that it eliminated any possibility of identifying fiber mechanical failure mechanisms. Figure 5.23 shows SEM images of broken fibers located along the centerline of IPS graphite-epoxy specimens burned for (a) 12, (b) 36 and (c) 60 s. In each case, the family of fibers became longitudinally thinner and developed needle-like shapes. Moreover, voids and cavities formed at the fiber ends in specimens burned for 60 s (Figure 5.24). Graphite/carbon fiber ends thinning is mainly caused by oxidation [23] occurring about a threshold temperature of 350-450°C [3]. Graphite/carbon fiber oxidation occurs at very low rates when the fibers are initially embedded in an epoxy matrix, since the char formed and deposited on the fiber

surfaces during burning acts as a protective layer that effectively stops the oxygen from reaching the fibers surface [8]. In addition, impurities like sodium can accelerate the oxidation process in graphite fibers [24]. These results suggest that extreme fire conditions leading to oxidation and/or sublimation of graphite/carbon fibers can render fractographic assessments of composite failure surfaces useless. In addition, any pyrolysis- or thermal-based approach aimed at removing char from burned graphite-epoxy fracture surfaces should be performed at temperatures near the matrix decomposition, and well below oxidation threshold and sublimation temperatures to avoid fiber thermal degradation.

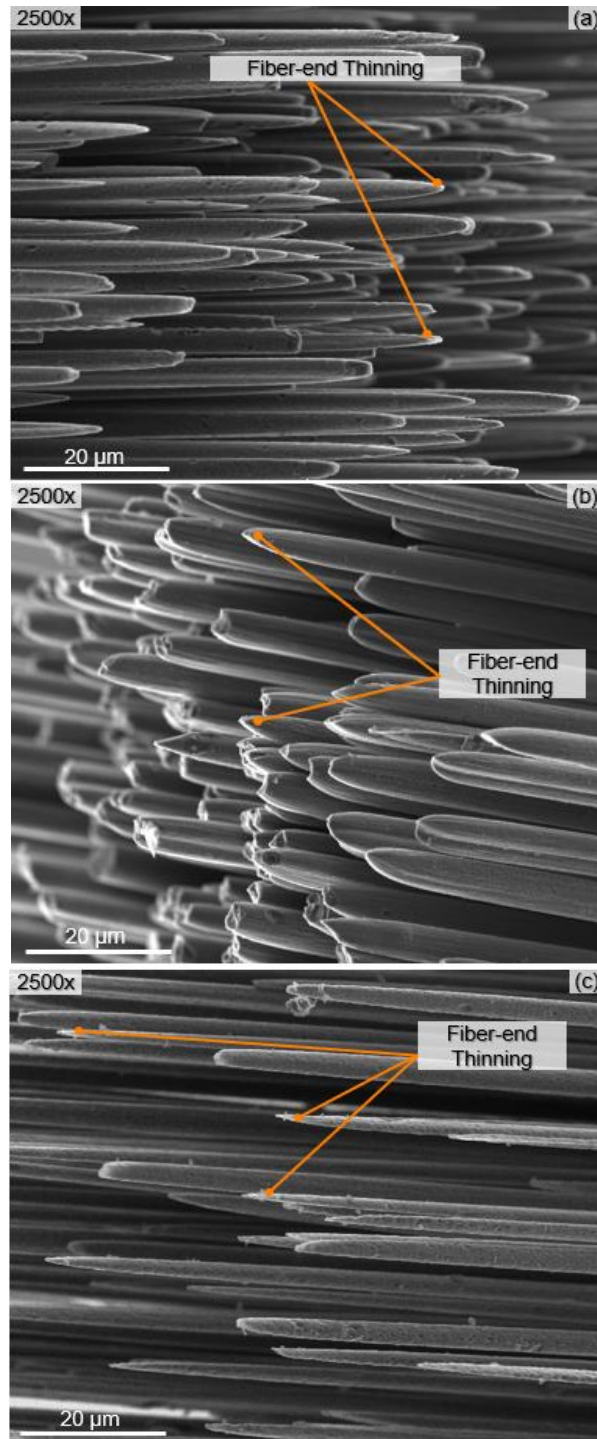


Figure 5.23 Fiber-end thinning of filaments located at the mid-plane of 16-ply Cytec Cycom 5215 T40-800 graphite-epoxy IPS specimens vertically burned for (a) 12, (b) 36 and (c) 60 s taken at WDs of 9, 15, and 10 mm, respectively.

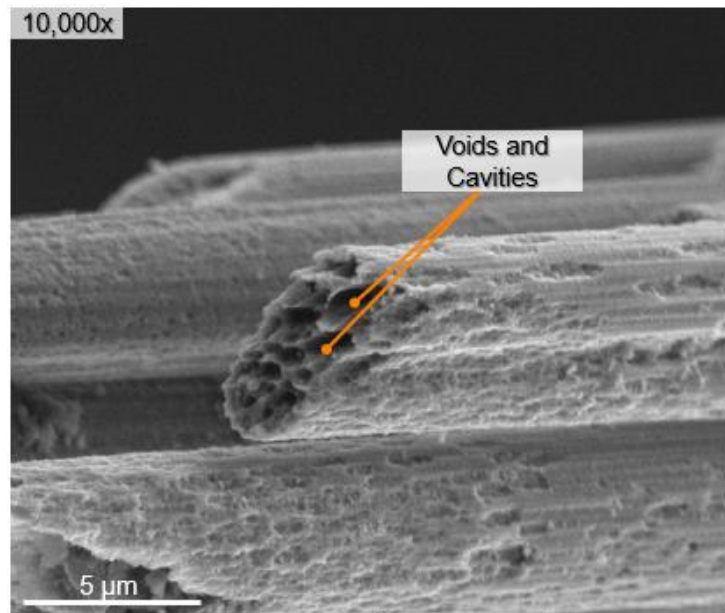


Figure 5.24 SEM image showing voids and cavities on a fiber from a 16-ply Cytec Cycom 5215 T40-800 graphite-epoxy IPS specimen burned vertically for 60 s.

5.2. Enclosed Horizontal Fire Testing of Cytec Cycom 5215 T40-800 Graphite-epoxy Specimens

5.2.1. UNC0 Specimens

Fire tests on horizontally-oriented 21-ply cross-ply Cytec Cycom 5215 T40-800 graphite-epoxy UNC0 specimens (lay-up: $[90/0/90]_7$) were performed for durations of 15, 45, and 75 s to assess the effects of specimen orientation and flame exposure time on fire damage formation. Three repeat horizontal fire tests were performed for each exposure time. The horizontally-oriented specimens typically experienced *lower* degrees of thermal damage than vertically-oriented specimens since a much smaller fraction of the total specimen volume is located above the tip of the flame. In each horizontal test, the UNC0 specimens self-extinguished as soon as

the applied flame was stopped. The local matrix decomposition, surface char, and soot were more severe over the lower outer ply surface exposed to direct flame; such damage was more pronounced for the 45 and 75 s fire tests. Unlike the case for vertical tests, no delamination or residual thickness increase occurred for all three fire exposure durations (*i.e.*, 15, 45, and 75 s). Figure 5.25 shows typical macro-scale images of the lower and upper surfaces of an UNC0 specimen before and after horizontal burning for 75 s. The lower surface of the specimen (Figures 5.25a, b) suffered matrix decomposition over the region exposed to direct flame. In contrast, the upper surface of the specimen (Figures 5.25c, d) was not appreciably affected by the fire.

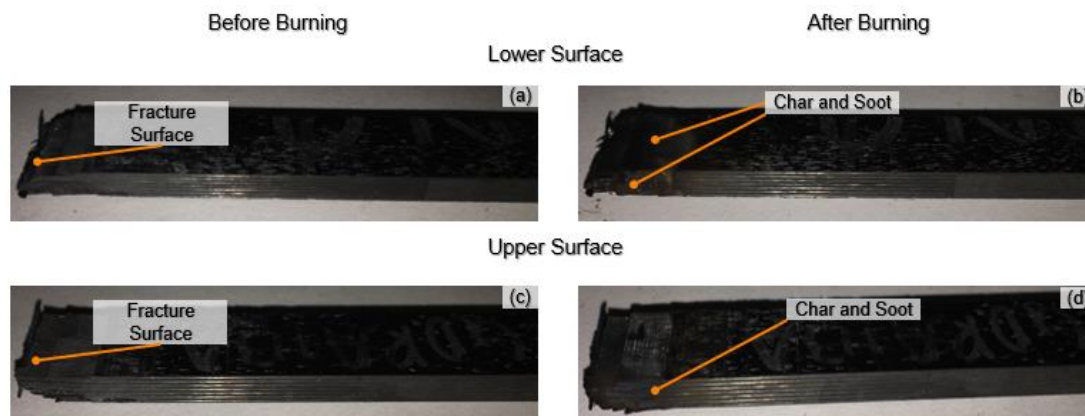


Figure 5.25 Pictures of a 21-ply cross-ply Cytec Cycom 5215 T40-800 graphite-epoxy UNC0 specimen; (a, c) before and (b, d) after horizontal burning for 75 s.

In the vertical fire test configuration, the specimens were held upside down into the flame (Figure 3.3a). In the horizontal fire test configuration, only the fractured edge of the bottom planar surface of the specimen was immersed into the flame (Figure 3.3b). The difference in fire damage extent and severity between UNC0

specimens used in vertical tests (Figure 5.2) and horizontal tests (Figure 5.25) may be due to differences in specimen in-plane and through-thickness thermal conductivities and other thermal properties. For example, the heat conduction parallel to the fibers will be much greater than through the ply thickness. The thermal conductivities of typical polyacrylonitrile (PAN)-based carbon/graphite fibers in the axial and radial directions are approximately 20 W/m·K and 0.32 W/m·K, respectively [3]. This compares to a value of 0.23 W/m·K for a typical epoxy matrix [3]. This suggests that, for horizontal tests, heat conduction in the outermost ply exposed to the flame will be greatest in the fiber direction. This may explain the greater degree of outer-ply matrix decomposition parallel to the plane in comparison to the through-thickness fire damage (*i.e.*, fire damage was more concentrated in the outermost ply). In contrast, for vertically burned specimens, the 0° fibers provide a more direct heat conduction path to the interior of the specimen, resulting in far more severe internal fire damage (melt dripping, matrix decomposition, delamination, explosive outgassing, *etc.*).

The amount of char formed at the fracture surface of UNCO specimens burned horizontally was different from specimens burned vertically. For horizontal tests, char was only deposited at the fire-exposed edge at the perimeter of the fractured surface. Figure 5.26 shows a typical SEM image of a horizontal UNCO specimen burned for 15 s. No large-scale cotton-candy-like char was deposited at the fractured fiber ends. Some char formed along the length of the extended fibers. SEM images of the fracture surface of UNCO specimens used in the 45 and 75 s horizontal fire tests have not yet

been performed due to the closure of the Texas A&M Material Characterization Facility during the COVID 19 period.

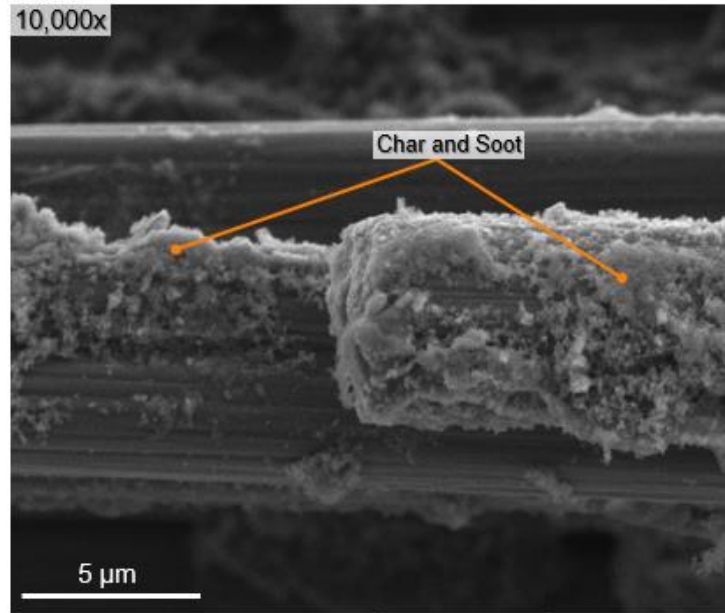


Figure 5.26 SEM image of the char and soot deposition at the fracture surface of a 21-ply cross-ply Cytec Cycom 5215 T40-800 graphite-epoxy cross-ply UNC0 specimen used on 15 s horizontal fire test.

5.2.2. SBS Specimens

Horizontal fire tests on 45-ply unidirectional Cytec Cycom 5215 T40-800 graphite-epoxy SBS specimens (lay-up: $[0]_{45}$) were performed for durations of 15, 45, and 75 s to assess the effects of specimen orientation and flame exposure time on fire damage formation. Three repeat horizontal fire tests were performed for each exposure time. Similar to horizontally-oriented UNC0 specimens, horizontally burned SBS specimens typically experienced much *lower* degrees of thermal damage than vertically-oriented SBS specimens since a much smaller fraction specimen volume is located directly into the flame. In each horizontal test, the SBS specimens self-

extinguished the instant the applied flame was stopped. Fire damage to horizontal SBS specimens was largely limited to large scale matrix decomposition concentrated near the fire-exposed surface, with little char/soot deposition and negligible residual thickness increase.

Figure 5.27 shows typical macro-scale pictures of the lower planar surface of a typical SBS specimen before and after horizontal burning for 75 s. The outermost ply exposed to direct flame (Figures 5.27a, b) sustained far more fire damage than did the interior plies. The lower edges of the fracture surface and lateral sides of the specimen also displayed proportionally more matrix decomposition than points more removed from the fire-exposed surface; this was particularly true for regions directly immersed in flame. In contrast, the upper outer ply and upper (unexposed) surface (Figures 5.27c, d) showed little fire damage at the proximity of the fracture surface.

As mentioned previously, during mechanical testing an individual half of a failed SBS specimen would sometimes longitudinally split into two $\frac{1}{4}$ -specimens due to high inter-laminar stresses induced in the three-point bending tests. These mating $\frac{1}{4}$ -specimens were subsequently clamped together during vertical and horizontal fire testing. After longer duration (36, 60 s) vertical fire tests, initially separated $\frac{1}{4}$ -specimens were bonded together after fire exposure. Conversely, in horizontal tests, the $\frac{1}{4}$ -specimens remained separated for all exposure times (15, 45, 75 s). Clearly, the relative orientation of any fissures and fracture surfaces relative to the flame can influence fire damage development. In addition, post-crash fire exposure has the

potential to bond aircraft composite fracture surfaces together in ways that might impede subsequent forensic analyses.

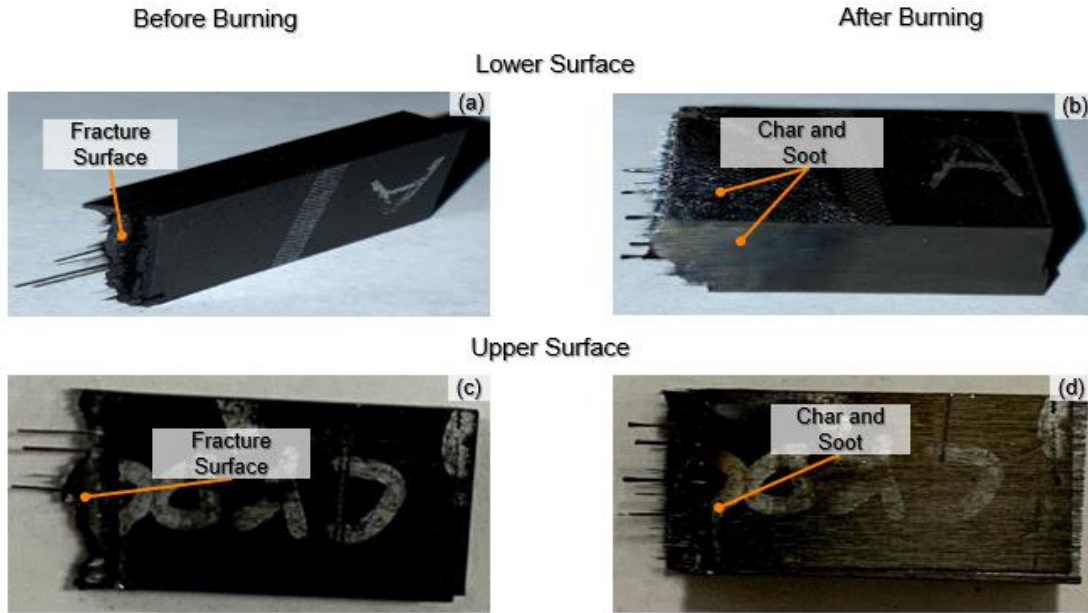


Figure 5.27 Pictures of a 45-ply unidirectional Cytec Cycom 5215 T40-800 graphite-epoxy SBS specimen; (a, c) before and (b, d) after horizontal burning for 75 s.

The degree of char formation and soot deposits on the fracture surfaces of horizontally-burned SBS specimens was much lower than that for similar specimens used in vertical fire tests (Figure 5.12). Figure 5.28 shows SEM images of the fracture surface of SBS specimens burned horizontally for (a) 15, (b) 45, and (c) 75 s. For specimens burned for 15 and 45 s, relatively minor amounts of char and soot residues formed on the fiber ends, and tensile failure regions and compressive chop marks were clearly visible (Figures 5.28a, b). For the 75 s tests (Figure 5.28c), many extended and recessed fibers were covered with melt dripping that obscured fracture surface features. In contrast to vertical fire tests where melt dripping by-products flowed

parallel to the fibers (due to gravity) and tended to accumulate at the filament ends, these by-products flowed parallel to the fracture surface in horizontal fire tests. Again, this suggests the relative orientation of both the flame and fracture surfaces affect composite thermal damage development, as well as post-fire forensic assessments.

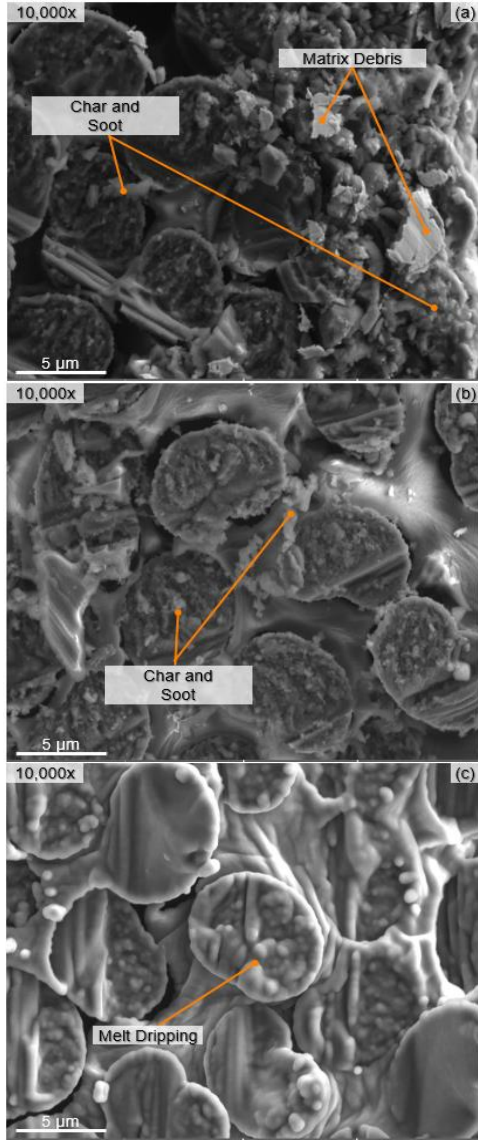


Figure 5.28 SEM image showing char and soot deposition at the fracture surface of 45-ply unidirectional Cytec Cycom 5215 T40-800 graphite-epoxy SBS specimens used for (a) 15, (b) 45, and (c) 75 s horizontal fire tests.

5.2.3. IPS Specimens

Horizontal fire tests on 16-ply Cytec Cycom 5215 T40-800 IPS specimens (lay-up: [45/-45]_{4S}) were performed for durations of 15, 45, and 75 s to assess the effects of specimen orientation and flame exposure time on fire damage formation. Three repeat horizontal fire tests were performed for each exposure time. Similar to horizontal testing of both the UNCO and SBS specimens, the angle-ply IPS specimens self-extinguished when the flame was stopped. The IPS specimens were positioned such that the midplane of the laminate was at the same height as the blue tip of the Bunsen burner flame (Figure 3.3b); the flame axis intersected the longitudinal axis of the specimen and lied in a vertical plane at the extreme edge of the fracture surface (*cf.*, “x” marks located in Figure 5.29b, d). Because of the highly irregular fracture surface, material at the laminate centerline and along the shortest lateral edge was slightly removed from the flame tip. Therefore, heat transfer at these two locations was primarily from convection of the hot air, gases, and smoke.

Figure 5.29 shows typical macro-scale images of the lower and upper surfaces of an IPS specimen before and after horizontal burning for 75 s. Soot and char were clearly visible on the lower (fire-exposed) surface of the specimen (Figures 5.29a, b). In contrast, no significant soot/char was observed on the upper surface of the IPS specimen (Figures 5.29c, d). In addition, no large-scale char or other fire damage were visible at the fractured fiber bundles protruding from the specimen fracture surface. The results from 15 and 45 s horizontal tests were consistent with those shown in Figure 5.29.

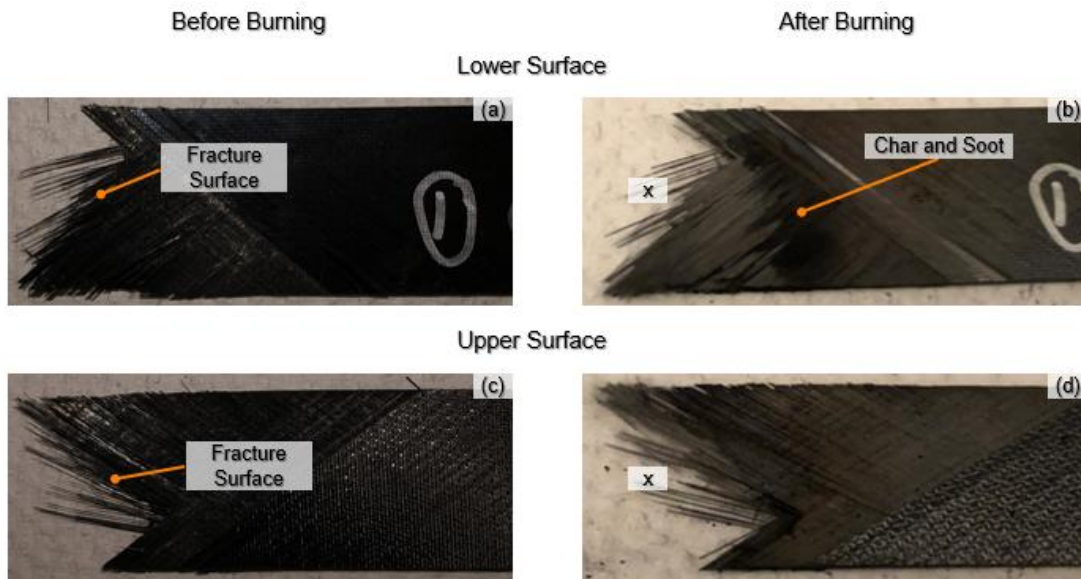


Figure 5.29 Pictures of a 16-ply Cytec Cycom 5215 T40-800 graphite-epoxy IPS specimen; (a, c) before and (b, d) after horizontal burning for 75 s; “x” denotes the approximate location of the axis of the vertical flame.

For *vertical* fire tests of IPS specimens, fibers located at the laminate centerline (location 2 in Figure 5.18a) suffered severe thermal degradation. In those cases, the matrix surrounding the fiber bundles was completely decomposed and individual filaments experienced substantial oxidation damage and thinning (Figure 5.23). For horizontal fire tests, however, fiber bundles located along the laminate centerline were not as adversely affected by fire exposure. Figure 5.30 shows SEM images of fiber bundles located at the centerline of IPS specimens horizontally burned for (a) 15, (b) 45, and (c) 75 s. For the 15 and 45 s fire exposures, individual fiber bundles remained encased in the epoxy matrix and there was little evidence of char formation (Figure 5.30a, b). For the 75 s tests, the epoxy matrix was largely decomposed but the individual fibers appeared to remain relatively intact. Moreover,

angled/slant fracture of individual filaments typical of in-plane shear failure was clearly visible (Figure 5.30c). It is obvious that horizontal testing of IPS specimens resulted in significant heat transfer due to convection that *bypassed* the specimen, resulting in far less thermal damage than for the case of vertical burning. These results suggest that under certain circumstances, post-crash fires may leave portions of composite aircraft structures relatively unaffected.

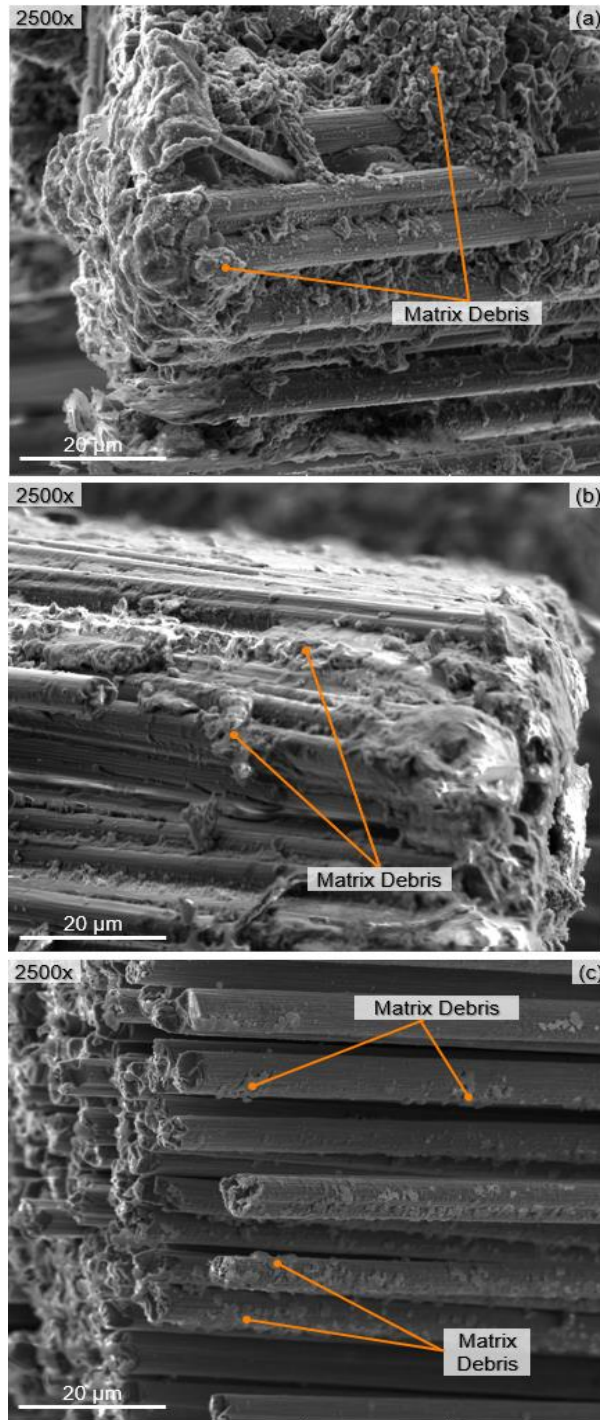


Figure 5.30 SEM images showing fiber tows from the centerline of 16-ply Cytec Cycom 5215 T40-800 graphite-epoxy IPS specimens after horizontal burning for (a) 15, (b) 45, and (c) 75 s.

5.3. Cone Calorimeter Testing of a Cytec Cycom 5215 T40-800 Graphite-epoxy Compression-after-impact (CAI) Specimen

In the preceding fire tests, failed UNCO, SBS, and IPS specimens were exposed to *direct* flame in draft-free cabinets to assess the effects of specimen geometry, lay-up, orientation, failure surface morphology, and flame duration on composite thermal degradation. As part of a corollary exercise, a single cone calorimetry test was performed to assess the effect of *indirect* fire exposure on thermal damage development in a 32-ply quasi-isotropic Cytec Cycom 5215 T40-800 graphite-epoxy plate (lay-up: [45/0/-45/90]_{4s}).

Prior to indirect fire testing, the composite plate was subjected to compression-after-impact (CAI) loading performed at Wichita State University [18]. During CAI testing, a 6 x 4 in² plate was first subjected to low velocity drop-weight normal impact with a spherical indenter to induce localized damage (fractured fibers, matrix cracks, ply-delamination, *etc.*) in and around a centrally-located impact site. The impacted specimen was then subjected to monotonically increasing in-plane compressive loading until failure. Laminate CAI failure, in this case, involved a combination of local fiber micro-buckling, fiber fracture, pure compressive fiber failure, matrix crushing, and other compressive instability related mechanisms that initiated at the impact site and propagated across the panel in a plane perpendicular to the loading direction. Unlike the UNCO, SBS, and IPS specimens, the failed CAI specimen was not separated into two distinct pieces after mechanical testing. Prior to cone calorimetry testing, a wet tile saw was used to machine a 4 x 4 in² sample from the

failed CAI specimen such that the impact site was centrally located, and the composite failure plane bisected two opposing edges of the sample.

During cone calorimetry testing, the 4 x 4 in² CAI sample was positioned horizontally *under* the cone (*i.e.*, indirect heat source) and a *through-thickness* heat flux of 50 kW/m² was applied continuously until the specimen self-extinguished. The specimen auto-ignited 81 s after initial heat flux exposure and self-extinguished 373 s after ignition. Figure 5.31 shows the CAI specimen after auto-ignition during cone calorimetry testing. During the test, large-scale matrix decomposition initiated at the upper heat-exposed surface of the specimen and eventually penetrated the entire thickness. After testing, no epoxy matrix or char was visible at the heat-exposed upper surface of the sample, *i.e.*, nearly complete matrix decomposition occurred (Figure 5.32a). The upper 45th ply of the composite appeared to consist of a blanket of *loose* bare graphite fibers (Figure 5.32b), which hindered SEM imaging of the upper surface. The unconfined loose arrangement of fibers at the composite outer surface made the broken and micro-buckled fibers at the CAI failure plane virtually *indistinguishable* from the surrounding fibers, based upon visual inspection. As an aside, *the inability to use visual inspections to precisely identify composite aircraft structural failure locations has the potential to seriously limit the efficiency of post-crash fire forensic analysis.*

During indirect fire testing, the CAI sample also experienced large-scale multi-ply-delamination along all four specimen edges that was most severe along the unloaded edges that intersected the composite failure plane (Figure 5.32c). In addition,

large amounts of melt dripping emanated from the edges of the specimen and flowed onto a horizontal metallic shelf located immediately below the cone calorimeter assembly (Figure 5.33). The melt dripping appeared to be a viscous tar-like substance that solidified after cooling; a melt drip sample was collected and sent to colleagues at Mississippi State University for carbon-hydrogen and nitrogen (C-H-N) and other chemical composition analyses. Such a substance may also have accumulated on extended graphite fiber ends during vertical burn tests on UNCO specimens (Figure 5.8), as well as been the source of interfacial bonding between pairs of mating ¼ SBS specimens subjected to vertical burning (as discussed in section 5.1.2). These issues remain to be fully explored.

During testing, the lower surface of the 32-ply CAI sample rested on a layered structure comprised of a thin aluminum foil, a low-density ceramic wool fiber blanket, and a stainless steel edge support frame. The lower surface of the specimen loosely adhered to the aluminum foil, likely due to melt dripping. After gently removing the foil, some matrix decomposition was apparent in the bottom 45 ply. Please note that detailed destructive micro-sectioning and ply-by-ply SEM inspection of semi-intact interior regions of the sample were not possible due to COVID-19 restrictions on laboratory access.



Figure 5.31 Cone calorimetry testing of a 4 x 4 in² 32-ply Cytec Cycom 5215 T40-800 graphite-epoxy CAI specimen.

In this research, the FAA was primarily interested in the effects of direct fire exposure on thermal damage development in mechanically-failed graphite-epoxy composites, as well as the establishment of strategies for char removal from burned aerospace composites. The vertical and horizontal direct fire tests on UNCO, SBS, and IPS specimens demonstrated that varying degrees of fire exposure can result in deposition of significant amounts of char and other fire by-products that can obscure salient aspects of composite fracture surface morphologies. Such deposits can impede fractographic and forensic assessments aimed at identifying underlying mechanical failure mechanisms. Although cone calorimetry was not widely employed in this work, it is clear that the application of a high heat flux to a graphite-epoxy composite can be used to completely decompose the epoxy matrix, leaving bare fibers with no

char. This suggests that char removal from previously burned composite specimens may be possible by subsequently subjecting them to sufficiently high temperatures or flame. If the fiber fracture surfaces are relatively unaffected by the prescribed thermal environment, this would potentially enable post-crash fire forensic analysis of large aerospace principal structural elements. This concept is consistent with those employed in ASTM standard matrix ignition tests [15] and efforts aimed at recycling carbon fibers from thermoset composites [16, 17]. While outside the scope of this thesis, one key challenge is to identify the optimal combination of heat source and environment that enables efficient char removal while minimizing thermal degradation to carbon or graphite fibers.

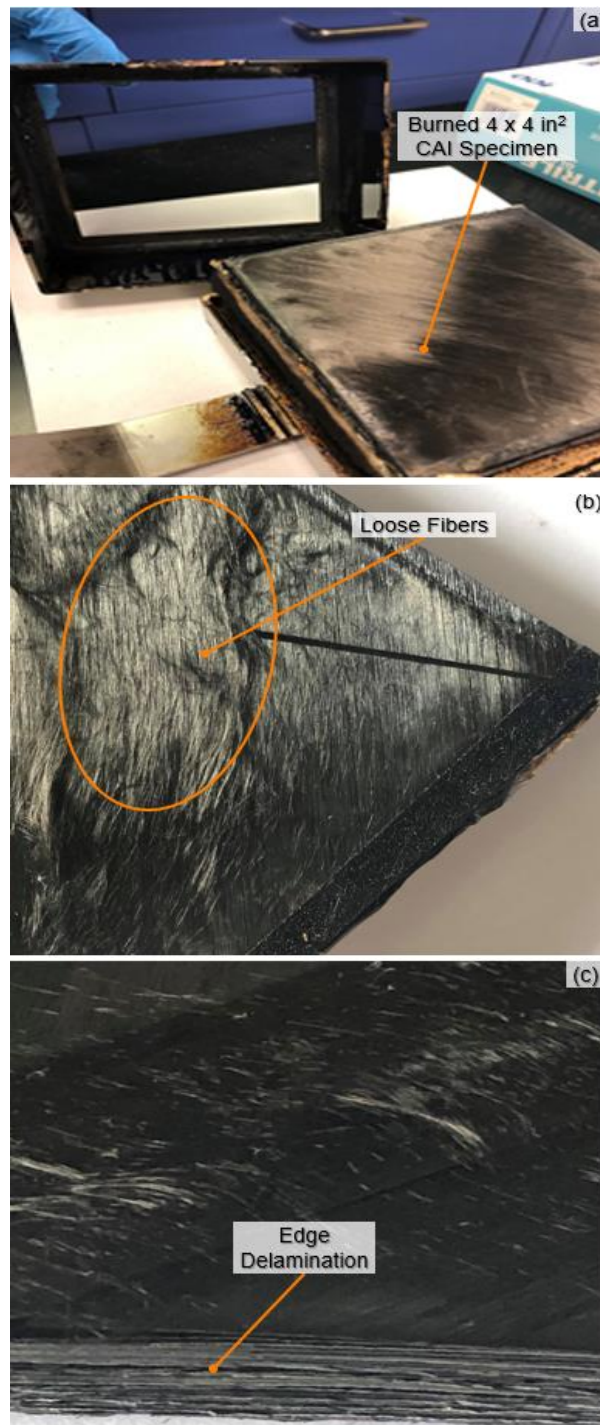


Figure 5.32 (a) 4 x 4 in² 32-ply Cytec Cycom 5215 T40-800 graphite-epoxy CAI specimen after cone calorimeter fire testing using a heat flux of 50 kW/m², (b) zoomed-in picture of the specimen showing loose fibers (c) zoomed-in picture of the specimen showing edge delamination.

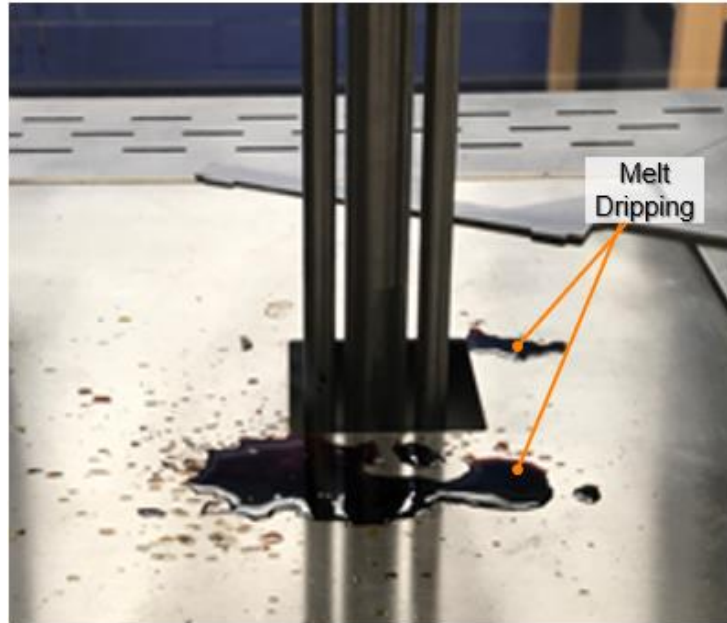


Figure 5.33 Melt dripping from the 4 x 4 in² 32-ply Cytec Cycom 5215 T40-800 graphite-epoxy CAI specimen.

6. SUMMARY AND CONCLUSIONS

The primary goal of this thesis is to investigate the effects of fire exposure on thermal damage development in mechanically-failed graphite-epoxy composites. This section contains a summary of key observations and research contributions associated with fire tests on unnotched compression (UNC0), short beam strength (SBS), in-plane shear (IPS), and compression-after-impact (CAI) specimens. Key findings from this research can facilitate post-crash fire forensic analysis of aerospace composite structures, as well as motivate future efforts aimed at char removal from burned composites.

A total of 21 vertical and horizontal fire tests were performed on mechanically-failed [90/0/90]₇ UNC0, [0]₄₅ SBS, and [45/-45]_{4S} IPS Cytac Cycom 5215 T40-800 graphite-epoxy specimens. In addition, a single cone calorimetry test was performed on a [45/0/-45/90]_{4S} CAI graphite-epoxy specimen. Visual inspection, and scanning electron microscopy of these specimens suggested that the specimen lay-up, orientation relative to the heat source (*i.e.*, vertical versus horizontal burning), and fracture surface morphology all had a significant influence on fire damage formation (*i.e.*, melt dripping, matrix decomposition, char, soot, matrix cracking, delamination, residual thickness increase).

For unidirectional continuous graphite fiber-reinforced epoxy plies subjected to fire, thermal damage due to heat conduction, combustion, and/or thermal deformation is highly dependent on the ply orientation relative to the flame. For unidirectional plies burned *perpendicular* to the fibers, the highly conductive graphite

fibers will conduct heat *parallel* to the fire-exposed surface (*e.g.*, along the fiber axis). This will promote decomposition and combustion of the epoxy matrix along the primary heat conduction path (*i.e.*, parallel to the fibers), with markedly less heat conduction and thermal damage through-the-thickness. In essence, plies with fibers oriented parallel to the heat exposed surface act like a thermal protection layer that can impede (slow) heat transfer to the interior of the specimen. This explains, in part, why horizontal burning of UNCO, SBS, and IPS specimens induced less thermal damage than did vertical burning. Similarly, the CAI specimen subjected to cone calorimetry testing sustained far more thermal damage near the heat exposed surface. As an aside, horizontal burning can also result in significant heat transfer due to convection of hot gasses and smoke that can *bypass* the specimen, which also leads to far less thermal damage than for the case of vertical burning.

In contrast, unidirectional plies burned *parallel* to the fiber axis will conduct heat *perpendicular* to the fire-exposed surface. For laminates, 0° plies aligned with the flame axis will conduct heat into the interior of the composite. This will occur more rapidly than if the fibers were oriented at 90° to the flame axis (parallel to the fire-exposed surface). Heat conduction in these 0° plies may promote formation of melt dripping, internal pockets of matrix decomposition, and surface char deposition. In addition, new matrix cracks and fissures may develop to accommodate explosive outgassing, resulting in a residual thickness increase (Figure 5.11). Mechanically-failed composites (such as the UNCO, SBS, and IPS specimens considered in this study) may contain fractured fiber ends that are either recessed within the specimen or

extended beyond the nominal fracture plane. After fire exposure, any melt dripping that occurs may accumulate on the extended filament ends (Figure 5.8) or coat the entire fracture surface (Figure 5.28c), depending on the fracture surface orientation relative to the flame.

Depending on the fire exposure time and temperature, any melt dripping or char deposits that form on the extended filament ends can completely obscure salient aspects of fiber fracture surface morphology. In some cases, however, the fracture surfaces of recessed fibers may be relatively unaffected by fire exposure, which may permit limited post-fire forensic analysis (*cf.*, Figures 5.5 and 5.14). Hence, *pre-examination* of fracture surfaces recovered from post-crash fires should be undertaken *before* attempting char removal. In contrast, fiber bundles that are excessively extended from the fracture plane are susceptible to extreme thermal degradation during fire exposure (*i.e.*, thinning, oxidation) which renders forensic analysis impossible (Figure 5.23). This is particularly true for specimens with highly irregular fracture surfaces (such as IPS specimens) that permit enhanced airflow and improved oxygen availability during burning.

Thermal damage development in mechanically-failed laminates can be compounded by the presence of different ply groupings in a given stack-up. For example, consider vertical burning of a $[90/0/90]_7$ UNC0 specimen (*i.e.*, the flame axis was parallel to the 0° plies). The 90° plies each acted like a thermal protection barrier that impeded (slowed) heat flow into the specimen. These plies conducted heat parallel to the fire-exposed fracture surface towards the lateral edges of the specimen,

leading to proportionally more char deposition around the specimen perimeter where the airflow and oxygen availability were greater. The 0° plies conducted heat into the interior of the composite, leading to melt dripping, matrix decomposition, char deposition, and explosive outgassing, as mentioned previously. Local differences in the coefficients of thermal expansion and thermal conductivities between the 0° and 90° plies resulted in fire-induced ply-delamination (Figure 5.9), matrix cracking (Figure 5.10), and discrete matrix cracking in the outer 90-degree plies (Figure 5.2c); these material discontinuities provided a pathway for matrix outgassing leading to potentially less residual thickness increase relative to unidirectional specimens (*i.e.*, SBS specimens). Similar arguments can be used to explain heat conduction, thermal deformation, and fire damage development in laminates with different ply groups.

Another point should be considered. The balance and symmetry of a given composite laminate may be destroyed by fire exposure. This is particularly true for horizontal burning and cone calorimeter tests, where an asymmetry in through-thickness ply properties arises from one-sided burning. The effect of the fire-induced loss of laminate balance and/or symmetry on thermal damage development was not part of this thesis and remains to be fully explored.

The composite lay-up and loading profoundly affect the fracture surface morphology and free surface area created during mechanical failure. Compression and transverse shear specimens loaded primarily parallel and/or perpendicular to the ply directions (similar to UNC0 and SBS specimens) may display more compact fracture surfaces with a minimum of free surface area creation. During fire exposure, thermal

degradation arises from a combination of burning of the combustible free surface area and heat conduction to the interior of the specimen. Carbonaceous char deposits forming on the fracture surface may act as a thermal barrier that further impedes oxygen transfer to the interior of the specimen and reduces the rate of thermal degradation until the onset of ply-delamination and/or matrix cracking. In contrast, angle-ply specimens that are loaded off-axis (similar to IPS specimens) commonly display extremely irregular fracture surfaces, ply-delaminations, and proportionally more free surface area creation. In general, specimens with more free surface area will promote better airflow and combustion during fire exposure, which can accelerate matrix decomposition and severe fiber thermal degradation for a given fire duration.

The total number of plies (*i.e.*, stack-up thickness) also affects the degree of damage for a given fire exposure. Thicker specimens with higher thermal mass may require greater heat input and longer fire exposure times to induce the same degree of thermal degradation as for thinner specimens. In addition, the local oxygen availability and airflow may be affected by the specimen fracture surface geometry. As mentioned previously, these factors may be exacerbated by variations in ply orientation and lay-up. Such considerations are crucial in the post-crash fire forensic analysis of aerospace composite structures.

Post-crash forensic analysis of composite aircraft structures typically focuses on principal structural elements. Here, a principal structural element can loosely be defined as a structural component (primary axial load carrying members such as critical wing spars flanges, longerons, carry-through structures, *etc.*) whose failure

would result in the catastrophic loss of an aircraft. These thicker structural components will typically be constructed with larger numbers of 0° plies. Hence, the [90/0/90]₇ UNC0 and [0]₄₅ SBS specimens are more consistent with principal structural elements than are the [45/-45]₄₅ IPS specimens. The IPS specimens are akin to aerospace laminates designed to carry torsional and/or shear loads (wing skins, spar webs, *etc.*).

In actual composite aircraft structures, principal structural elements are typically designed to carry high axial or bending loads. As a consequence, they are commonly constructed of *thick* composite laminates (40-100+ plies) containing a majority of 0° plies, somewhat fewer ±45° plies, and a minimum of 90° plies (of course, other ply groupings are possible). Similar to the UNC0, SBS, and IPS specimens considered in this research, discrepancies in principal structural element local ply properties, lay-up, and loading may influence mechanical damage development during catastrophic failure, as well as thermal degradation due to a post-crash fire. The mechanisms responsible for composite thermal degradation during an actual aircraft fire will also be comparable to those discussed here. To the author's knowledge, *this research is the first to investigate i) the effects of fire exposure on mechanically-failed continuous graphite fiber-epoxy laminates, and ii) the influence of specimen lay-up, orientation, and fracture surface morphology on different thermal degradation mechanisms in aerospace composites.*

Fuel-fed post-crash fires can be high-intensity long duration phenomena [5, 7, 14, 25] that are distinct from the small-scale fire tests on ASTM standard composite

specimens performed in this work. Nonetheless, this research represents an important first step in the development of a coherent strategy for the FAA post-crash forensic analysis of composite aircraft structures. Actual post-crash fires can burn and then smolder for hours after initial ignition [25], resulting in the deposition of massive amounts of char and other fire by-products (including those due to paint, hydraulic fluid, foam cores, *etc.*) on the composite failure surfaces. Such deposits can form a thick barrier that protects the underlying composite from further thermal degradation but completely masks the composite failure surfaces. In order to facilitate post-crash fire forensic analyses of composite aerospace structures, a combination of thermal, physical and/or chemical approaches for char removal must be developed. Potential techniques may include combinations of specimen liquid nitrogen dipping, elevated temperature exposure near the matrix decomposition temperature (in inert and oxidative atmospheres), ultrasonication, micro-machining, solvent soaking, *etc.* In extreme cases, post-crash fires can completely destroy all forensic evidence necessary for accident reconstruction.

In the future, large-scale open pool fire experiments (or similar tests) should be performed on fractured skin-stiffened semi-monocoque aerospace composite structures and/or principal structural elements. These tests will enable characterization of thermal degradation in realistic composites, as well as development of viable in-field strategies for char removal from commercial and general aviation aircraft.

REFERENCES

- [1] Kabche, J. P., 2006, "Structural testing and analysis of hybrid composite/metal joints," Electronic Theses and Dissertations, 274, the University of Maine.
- [2] Botelho, E.C., Silva, R.A., Pardini, L.C. and Rezende, M.C., 2006, "A review on the development and properties of continuous fiber/epoxy/aluminum hybrid composites for aircraft structures," *Materials Research*, 9(3), 247-256.
- [3] Mouritz, A. P., and Gibson, A. G., 2006, Properties of Polymer Composite Materials, Solid Mechanics and its Applications, The Netherlands.
- [4] Mouritz, A.P., 2003, "Fire resistance of aircraft composite laminates," *Journal of materials science letters*, 22(21), 1507-1509.
- [5] Federal Aviation Administration, 2007, "Special conditions: Boeing model 787-8 airplane; composite wing and fuel tank structure-fire protection requirements," Federal register 72(196), FR doc number: E7-20031. Available at: <https://www.federalregister.gov/documents/2007/10/11/E7-20031/special-conditions-boeing-model-787-8-airplane-composite-wing-and-fuel-tank-structure-fire> (Accessed April 2020).
- [6] Zhang, Z., 2010, "Thermo-mechanical behavior of polymer composites exposed to fire," PhD Dissertation, Virginia Polytechnic Institute and State University.
- [7] Chen, Z.-M, "Composite failure analysis after post-crash fire," FAA, PowerPoint Document, presented to Mississippi State University, June 26, 2018, Miss. State, MS, USA.
- [8] Mouritz, A.P. and Mathys, Z., 2001, "Post-fire mechanical properties of glass-reinforced polyester composites," *Composites Science and Technology*, 61(4), 475-490.
- [9] Mouritz, A. P., Gardiner, C. P., Mathys, Z., and Townsend, C. R., "Post-fire properties of composites burned by cone calorimetry and large-scale fire testing," **ID-1273**.
- [10] Mouritz, A., Feih, S., Kandare, E., Mathys, Z., Gibson, A., Des Jardin, P., Case, S., and Lattimer, B., 2009, "Review of fire structural modelling of polymer composites," *Composites Part A: Applied Science and Manufacturing*, 40(12), 1800-1814.
- [11] Wood, R. H., and Sweginnis, R. W., 2006, Aircraft Accident Investigation, "Fire investigation. "Available

at:https://www.marvgolden.com/downloads/dl/file/id/99/aircraft_accident_investigation_book_excerpt.pdf (Accessed April 2020).

[12] Federal Aviation Administration, 2009, Advisory Circular 150/5200-12C, “First responders' responsibility for protecting evidence at the scene of an aircraft accident/incident.”

[13] Rakow, J. F., and Pettinger, A. M., 2007, Failure Analysis of Composites: A Manual for Aircraft Investigators, Exponent.

[14] Stanley, D., and Oztekin, A., “Composite failure analysis after post-crash fire,” FAA, PowerPoint Document, presented to Mississippi State University, May 9, 2019, Miss. State, MS, USA.

[15] ASTM Standard D2584-18, 2018, “Standard test method for ignition loss of cured reinforced resins,” ASTM International, West Conshohocken, PA, doi: 10.1520/D2584-18.

[16] Fernández, A., Lopes, C.S., González, C., and López, F.A., 2018, “Characterization of carbon fibers recovered by pyrolysis of cured prepregs and their reuse in new composites,” Recent Developments in the Field of Carbon Fibers, 103-120.

[17] Yang, Y., Boom, R., Irion, B., Heerden, D-J., Kuiper, P., and de Wit, H., 2011, “Recycling of composite materials,” *Chemical Engineering and Processing*, 51(2012), 53–68.

[18] Man, M., 2012, “Cytec Cycom 5215 T40-800 unitape Gr 145 33% RC: Qualification material property data report,” NCAMP test report number: CAM-RP-2010-048 Rev N/C.

[19] Horner, A., 2000, Aircraft Materials Fire Test Handbook, Federal Aviation Administration, DOT/FAA/AR-00/12, Washington, D.C. 20591. Available at: <http://www.tc.faa.gov/its/worldpac/techrpt/ar00-12.pdf> (Accessed August 2020).

[20] Babrauskas, V., and Peacock, R.D., 1992, “Heat release rate: The single most important variable in fire hazard,” *Fire Safety Journal*, 18(3), 255-272.

[21] Beyler, C., Croce, P., Dubay, C., Johnson, P., and McNamee, M., 2017, “Oxygen consumption calorimetry, William Parker: 2016 DiNenno Prize,” *Fire Science Reviews*, 6(1).

[22] Sinha Ray, S., Kuruma, M., 2020, Halogen-Free Flame-Retardant Polymers, Next-generation Fillers for Polymer Nanocomposite Applications, Springer.

[23] Greenhalgh, E., Failure Analysis and Fractography of Polymer Composites, Woodhead Publishing in Materials, Cambridge, UK.

[24] Susshol, B., 1980, "Evaluation of micron size carbon fibers released from burning graphite composites," NASA Contractor Report 159217.

[25] Wright, M. T., Luers, A. C., Darwin, R. L., Scheffey, J. L., Bowman, H. L., Davidson, R. A., and Gogley, E. J., 2003, "Composite materials in aircraft mishaps involving fire: A literature review, " Naval Air Warfare Center Weapons Division China Lake, CA 93555-6100.